LUND UNIVERSITY
Faculty of Science

Handling of long DNA – applications and polymer physics

Alexandra Kühnlein

Thesis submitted for the degree of Master of Science
Project duration: Nine months

Supervised by Prof. Dr. Jonas Tegenfeldt and
Dr. Jason Beech

Department of Physics
Division of Solid State Physics
May 2016

Abstract

This thesis provides a proof of principle that deterministic lateral displacement (DLD) can be used to spatially separate DNA molecules by size. In order to achieve high separation quality, the pressure range, *i.e.* flow velocity has to be chosen carefully. The experiments were conducted in DLD devices fabricated in PDMS using soft lithography methods. Fluorescently labeled DNA molecules were transported through the device by pressure driven flow. The separation results were determined from and the separation result was recorded optically at the outlet. Both tested devices, with a critical diameter D_c of 0.64 μm and 0.75 μm respectively, showed capable of separating <10 kbp from 48.5 kbp DNA molecules with a separation quality of $\simeq$ 94%.

Acknowledgments

First of all, I would like to thank Prof. Jonas Tegenfeldt for the opportunity to work on such an interesting project and for letting me experience the friendly, cooperative and constructive research environment he created in his group. I am grateful for his constant help and support, the countless fresh ideas he provided and especially for his astounding enthusiasm for science which I found very inspiring.

Secondly, I want to express my gratitude to Dr. Jason Beech for all the invested time and his dedicated support during the whole project. He teached me everything I needed to know in the lab and as the project carried on he proved himself to be indispensable because of his unbeaten problem-solving abilities. I want to thank him especially for all the helpful input and discussions we had on the project.

Also, I would like to thank Rebekah Kim for her support in the lab and her lovely company during lunches, Bao Ho Dang for designing and fabricating the silicon moulds for the DLD devices and the rest of the Tegenfeldt group for interesting and fruitful meetings and a relaxed working atmosphere.

Finally, I want to thank my family and friends for the belief they have always shown in me, for their ceaseless encouragement and for the all the times they had to be patient and sympathetic.

List of Figures

List of Abbreviations and Acronyms

BME	β-mercaptoethanol
bp	base pair
D_c	Critical diameter
DI water	Deionized water
DLD	Deterministic lateral displacement
DNA	Deoxyribonucleic acid
EDTA	Ethylenediaminetetraacetic acid
FJC	Freely-jointed chain
NA	Numerical aperture
PDMS	Polydimethylsiloxane
PFGE	Pulsed-field gel electrophoresis
Pe	Peclet number
Re	Reynolds number
TAE	TRIS-acetat-EDTA buffer
WLC	Worm-like chain

Contents

Chapter 1

Introduction

In molecular biology, but also in biophysical, biochemical and medical contexts, the length-based separation of DNA molecules is a crucial step during many experiments. It can be necessary either as preparatory step or for the final sample characterization or purification.

Today's standard method for the length-based separation of DNA molecules is gel electrophoresis. It uses an electric field to pull the charged DNA molecules through a gel matrix which results in spatial separation. However, gel electrophoresis has several major drawbacks. The length and concentration limits under which it can be operated are stringent. Only molecules shorter than roughly 40,000 base pairs can be separated and even under optimal conditions, at least 20 pg of DNA are required for detection [1]. This corresponds to $\sim 10^5$ - 10^6 DNA molecules. Furthermore, after the separation the DNA molecules are contained in a gel and the recovery can be laborious [2].

During the last two decades the field of microfluidics has been evolving rapidly. The benefits of microfluidic systems are that they are capable of handling very small sample volumes, allow single cell analysis, provide good sample control and are typically easy to handle and fabricate. This makes microfluidic systems especially suited for biological applications and indeed, in recent years microfluidics-based bioanalytical systems havebeen advancing [3, 4]. Recalling the current limits of length-based DNA separation, it is apparent that when working in the microfluidic regime, the availability of DNA separation methods is restricted. Simultaneously, it is obvious that microfluidic approach would also be a convenient solution to the DNA separation problem. Indeed, there are various mirofluidic particle separation methods available which might also be suitable for theseparation of DNA molecules. Nice articles reviewing the different methods are provided by Lenshof and Laurell, [3] and Sajeesh and Sen, [5].

In 2000, Han and Craighead, [2], demonstrated that entropic trap arrays in microchannles can be used for DNA separation. Although, their approach permitted only batch separation, which means that the DNA molecules arrive at the same final position but at different times. In 2004, Huang *et al.*[6] introduced a new particle separation method called Deterministic Lateral Displacement (DLD). In DLD, particles travel through an obstacle array and arrive at different final positions depending on their size. Already in the original publication, Huang *et al.* demonstrated that their method can be used to separate DNA molecules by length. However, both Han and Craighead, and Huang *et al.* use an electric field to pull the DNA through their respective arrays. As DNA separation is typically needed in sample pre- or post-processing, the separation process 1

should be easily compatible and integrable with other devices and techniques. Therefore, use of an electric field which requires additional equipment is undesirable. Quite recently, Chen *et al.* [7] demonstrated that DLD operated with pressure-driven flow can be used to concentrate chemically compacted DNA molecules.

In this work, the length-based separation of DNA in a DLD devices using pressure-driven flow is investigated. For the experiments, three viral DNA samples of different length are probed in two DLD devices with different separation ranges. The separation results are analyzed thoroughly and it is furthermore discussed how the DNA's polymeric nature might affect its performance in the microfluidic device.

Many applications of the proposed approach regard sample purification. Two concrete examples shall be given here. Firstly, it would easily be possible to separate long and short DNA pieces after the application of restriction enzymes yielding a purified sample of long DNA pieces which can be used for next-generation sequencing techniques as optical mapping. Secondly, a DNA sample which was stained with a non-binding-enhanced fluorescent dye can be cleaned of the left over dye molecules to reduce the fluorescent background and facilitate imaging. In both cases the simple method would result in an enormous improvement.

However, one can also think of one long-term research goal: the development of an integrated lab-on-a-chip system which can perform single-cell DNA analysis. The envisioned system is capable of taking a single cell or a complete sample (such as a conventional blood sample) as input and output characteristic information about the DNA of the inserted sample or molecule. For such a system, cell-lysis, DNA extraction and separation as well as optical mapping [8] have to be integrated on one chip. One of the main components of such a lab-on-a-chip system could be a DLD device responsible for the separation of the DNA molecules into the nanochannels. Single-cell DNA analysis would be a breakthrough in molecular biology, would have a great impact on medical applications and could tremendously simplify today's diagnosis. To give an example: nowadays, if a patient has a rare bacterial infection it can take up to three weeks until the patient's sample is cultivated and the DNA of the bacterium can be identified. With the suggested lab-on-a-chip system, the identification would be finished within a few hours and only very little sample from the patient would be required, a few μL suffice.

In the field of biophysics, it is often necessary to consider ethical issues and the impact of the conducted research. However, in this project only viral DNA which is extracted from bacteria is used. This type of sample does not underlie any ethical restrictions and the usage is generally seen without misgivings. Nevertheless, it is of course important to place every experiment and study in the grand picture since even if every small step is acceptable, their combination might not be so. One of the ultimate research aims in this field, to develop chips for single-cell DNA analysis, is certainly a questionable issue. Yet, the ongoing projects are focusing on using the newly developed techniques to improve diagnosis in medicine especially for rare disease and in developing countries. This research could lead to such enormous improvements for mankind and can at least at this point be seen without ethical concerns.

Chapter 2

Theoretical background

This chapter will introduce the theoretical concepts from fundamental physics which are required to comprehend the experimental approach and results as described in the following chapters. An overview of DNA polymer physics, fluorescence microscopy and fluidics theory focusing on microfluidics will be provided.

2.1 DNA polymer physics

Deoxyribonucleic acid, DNA, is a polymeric biomolecule. It is contained in any living organism as well as in some virus types and carries all genetic information. DNA is composed of a backbone which consists of alternating, covalently bound five-carbon sugar deoxyribose and phosphate groups.

Typically, two sugar-phosphate backbones are intertwined and form a characteristic double-helical structure. To every sugar group of the backbone one of the four nitrogen-based nucleic acids, Adenine (A), Cytosine (C), Guanine (G) and Thymine (T) is bound. Each of those four nucleic acids, can bind complementary to one other nucleic acid, such that two base pairs, A-T and G-C can be formed within the double helix. Each base pair contributes 0.34 nm to the length of a DNA molecule. The hydrodynamic diameter of the double helix is approximately 2.5 nm [10]. A sketch of a DNA strand is shown in Figure 2.1.

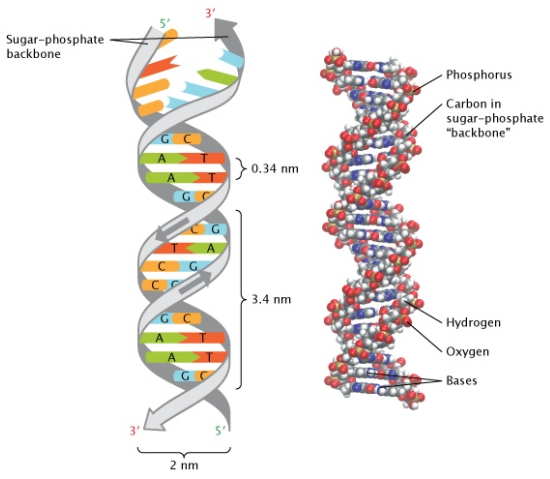

Figure 2.1: (*Left*) Schematic depiction of a DNA strand, showing the double helical structure formed by the backbone and the complementary base pairs. (*Right*) Molecular level depiction. Reprinted with permission from [9]. Copyright 2013 Nature Education.

DNA encodes information by the distinct sequence of the nucleic acids. However, different organisms do not only vary in the order of the nucleic acids, but show also differently sized genomes. Some typical genome sizes for various organisms are given in Table 2.1.

Table 2.1: Overview of genome sizes of different organisms, [11].

Organism	Genome size
Mammal (human)	3.2 Gbp
Insect (bee)	236 Mbp
Plant (*Arabidopsis thaliana*)	157 Mbp
Yeast (*S. cerevisiae*)	12.1 Mbp
Bacterium (E-coli)	4.6 Mbp
Virus (λ-phage)	48.5 kbp

2.1.1 Polymer theory of free DNA

Due to the DNA's complicated chemical composition and the importance of thermal fluctuations on the molecular level, it is impossible to find an exact, three-dimensional, time-dependent description of its state. Therefore, different models have been developed to explain basic properties of a complicated polymer such as DNA. The simplest approach is the freely-jointed chain (FJC) model, which assumes that the polymer consists of N stiff, rod-like monomers of length a connected by perfectly flexible joints. Since the angles between the joints are uncorrelated in the FJC model their orientation is determined by a three-dimensional random walk which results in a random coil arrangement [12]. The FJC model neglects the spatial extension of the composing monomers and therefore disregards steric hindrance [13]. The contour length, which is the length at maximum possible extension is defined as

$$L = aN. \tag{2.1}$$

Generally, the radius of gyration is defined as the mean square distance of all elements to the center of mass and is a commonly used estimate for the spatial extension of irregular shaped particles. For the random DNA coil the radius of gyration is given by

$$R_{\mathrm{FJC}} = \frac{a\sqrt{N}}{\sqrt{6}}. \tag{2.2}$$

A more intricate and realistic characterization than the FJC model is provided by the worm-like chain (WLC) model. In contrast to the FJC model, it is based on a continuous description of the polymer chain. Within the WLC model, DNA is described as semi-flexible polymer which means it exhibits flexible behavior at length scales close to the polymer size and is rigid on the scale of one monomer unit. The limit of those regimes is defined as the persistence length P, the length scale over which transformational correlations are lost. For double-stranded DNA, P is typically around 50 nm [13, 14].

However, even though both models yield acceptable results, they are coarse simplifications. For real DNA molecules, the same volume can only be occupied once (excluded volume effect), the polymer chain can not intersect with itself and monomers can interact electrostatically. To compensate for these effects, the effective width, w_{eff} is introduced, which is a measure for the width of the chain taking physical and electrostatic interactions into account [8, 15]. The effective width, as well as all other physical parameters

describing DNA, is highly dependent on the ionic strength. At low salt concentration ($\sim$ 5 mM) the effective width is as low as 5 nm while it increases to around 20 nm at high salt concentration ($\sim$ 100 mM) [15].

Considering DNA free in solution, entropic forces will cause the volume of the DNA coil to minimize whereas steric effects will force the DNA coil to expand. Balancing between those, a DNA molecule forms a coil whose radius, R_F, can be derived to be, [8, 15],

$$R_F \sim (w_{\text{eff}} 2P)^{\frac{1}{5}} L^{\frac{3}{5}}. \tag{2.3}$$

This radius, R_F, is typically referred to as Flory radius or radius of gyration. Note that taking the electrostatic and steric effects into account results in a larger coil since the radius of the coil scales now with $N^{\frac{3}{5}}$ in contrast to $N^{\frac{1}{2}}$ in the simple model.

2.1.2 Polymer theory of confined DNA

DNA confinement occurs if DNA is forced into a space in which at least one dimension is smaller than the radius of gyration of a free coil. Polymer statistics are changed depending on the degree of confinement which is governed by the relation of the geometric average of the confining channel and the persistence length. The geometric average of the channel D_{av} is defined as $D_{av} = \sqrt{D_1 D_2}$ with D_1 and D_2 being the width and height of a rectangular channel respectively.

De Gennes, [16], proposed that if the geometric average of the channel is much bigger than the persistence length, the confined DNA can be seen as linearly arranged non-interacting blobs inside which subchain behaves just as in free solution. Since the channel dimensions are still larger than the persistence length, the DNA can partly fold and arrange into a coil, which in turn means that the behavior is dominated by excluded volume effects [8, 17]. A sketch of a DNA molecule under confinement in the de Gennes regime is shown in Figure 2.2 (*center*). In the de Gennes regime, the length of the confined DNA molecule, L_z, is given by, [18],

$$L_z \simeq L \left(\frac{P w_{\text{eff}}}{D_1 D_2} \right)^{\frac{1}{3}}. \tag{2.4}$$

Under stronger confinement, *i.e.* if the geometric average of the channel is much smaller than the persistence length, DNA statistics are well described by Odijk's theory in which the chain stiffness is the dominating component [19]. Due to the strong confinement, the DNA is no longer able to change its configuration by thermal fluctuations and gets therefore elongated along the channel axis, as sketched on the right of Figure 2.2 (*right*). Odijk suggests that DNA can thus be seen as consisting of linked completely rigid elements of length λ, the deflection length.

Notably, in both theories the end-to-end distance of the confined DNA molecule is directly proportional to the number of base pairs N, *i.e.* the contour length L. However, neither of the two theories provides results which correspond well to experimental results [8, 17]. This is most likely because typical experimental conditions, with a persistence length of $\approx$ 52 nm for double stranded DNA and nanochannel dimensions ranging from 50-200 nm, lie inbetween the two extremes which can be theoretically well described. Current research is investigating an additional regime, between the de Gennes and Odijk regime, which has been titled extended de Gennes regime [17, 20, 21, 22].

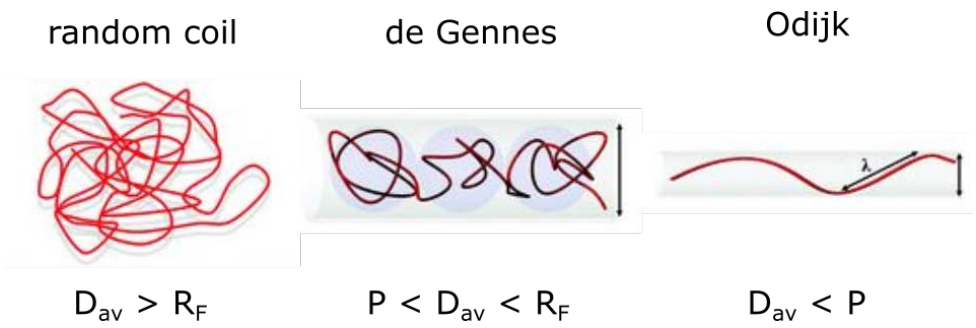

Figure 2.2: Illustration of the three main different regimes of DNA confinement. (*Left*) DNA as free coil as formed by three-dimensional random walk. (*Center*) De Gennes regime where DNA is capable of folding and developing blobs in which the random walk statistics are valid. (*Right*) Odijk regime where DNA is stretched and alternating between the channel walls. Sub-chains with deflection length λ are assumed to be completely rigid. Figure adapted from [8].

2.1.3 DNA in fluid flow

The problem of the dynamical deformation and elongation of DNA molecules in fluid flow has been subject to a remarkable number of studies in the field of polymer physics [23, 24, 25, 26, 27, 28]. This is an indication of how complex the problem is. In the following, a brief introduction to the effects of shear stress induced by hydrodynamic flow in DNA molecules will be given.

Generally, a DNA molecule under fluid flow deforms if the hydrodynamic friction across the molecule is larger than the entropic forces which cause the random coil formation [29]. This leads to an extension parallel to the hydrodynamic flow. Smith *et al.* [30] demonstrated that the extension of a DNA molecule is proportional to the exponential of the applied drag force, $\frac{\langle x \rangle}{L} \sim \exp(F)$. Perkins *et al.*, [27], showed that the extension of DNA molecules in fluid flow scales in the ensemble average with the square root of time, $\frac{\langle x \rangle}{L} \sim t^{1/2}$. However, it is important to mention that due to the initially random conformation of a DNA coil, the rate of stretching can be substantially different for each DNA molecule [27, 29].

Furthermore, the relaxation time of a stretched molecule can be considered. The terminal relaxation time, τ_{DNA}, which is governed by the thermal fluctuations which bring the DNA molecule back into the random coil conformation, can be estimated by [23],

$$\tau_{\mathrm{DNA}} \simeq \frac{2\eta_S R_F^3}{k_B T}, \tag{2.5}$$

where η_S is the viscosity of the solvent and R_F is the Flory radius of the undisturbed DNA coil.

Moreover, Bakajin *et al.*, [31], proved that the extension rate for a confined DNA molecule increases with the degree of confinement whereas its relaxation time decreases.

2.2 Fluorescence Microscopy

Fluorescence is a physical phenomenon which is defined as the emission of light by a substrate due to a singlet-singlet spin-allowed electronic transition. It occurs when electrons

in the substrate have previously been excited by the absorption of light [32]. Due to energy conservation, the emission wavelength, λ_{em}, has lower energy than the excitation wavelength, λ_{em}, *i.e.* $\lambda_{\text{em}} < \lambda_{\text{ex}}$. This difference is called Stokes shift and is due to the amount of energy which is lost during the non-radiative, vibrational relaxation into the lowest level of the excited state which typically occurs before the molecule relaxes electronically. Figure 2.4 shows a typical excitation and emission spectrum of a fluorescent dye.

In epi-fluorescence microscopy, fluorescence is used to create an image. A sample to which fluorescent molecules have been attached is illuminated with the according excitation wavelength λ_{ex} to transfer the molecule into an excited state. Upon de-excitation, those molecules will emit light with wavelength λ_{em} which can then be observed. A schematic setup of an epi-fluorescence microscope is shown in Figure 2.3.

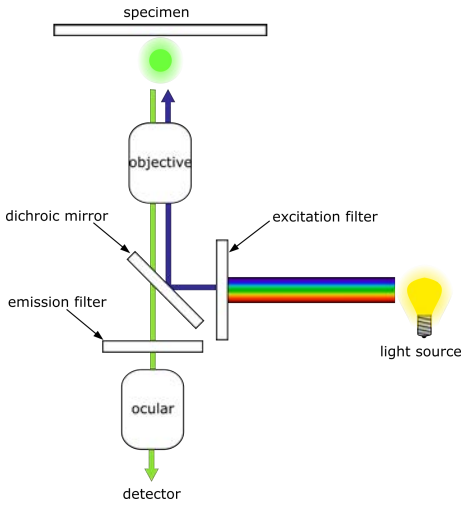

Figure 2.3: Sketch of an epi-fluorescence microscope as described in the text. Figure adapted from [33].

The light source, typically a xenon arc or mercury-vapor lamp, provides a continuous spectrum in the visible range. The supplied light passes through an excitation filter which allows only light close to the excitation wavelength to penetrate. The following dichroic mirror is designed such that it reflects light below a certain wavelength but transmits wavelengths above it. Light close to the excitation wavelength gets reflected and directed into the objective which focuses the beam onto the specimen. There, fluorescent molecules are excited and subsequently emit light of the emission wavelength isotropically. Thus, a fraction of the emitted light and some elastically scattered excitation light re-enter the light path in the microscope. Only the light of the emission wavelength contains information about the sample. Therefore, again by passing through a dichroic mirror and the emission filter other wavelengths are filtered out. The excitation and emission filter as well as the dichroic mirror are contained in the so-called filter cube, which is specific to a certain fluorescent molecule since it defines the range for λ_{ex} and λ_{em}. An objective is usually characterized by the magnification and the numerical aperture, NA, which is a measure for the angle in which the objective can capture photons, defined as,

$$\text{NA} = n \sin\theta, \tag{2.6}$$

where n is the refractive index of the medium in between sample and objective and θ is the half-angle of light cone which can be captured.

The enormous advantage of epi-fluorescence microscopy is that, due to the specific labeling and the adjusted filters it allows to purely image the desired sample. Furthermore, the non-fluorescent background is filtered out and a better signal-to-noise ratio is ensured. The major disadvantage is that fluorescent molecules have to be attached to the sample,

which changes its native state and might alter the behavior. To achieve good results using epi-fluorescence microscopy a fluorescent dye with high quantum yield, an objective with high NA and a suitable camera should be used.

2.2.1 Fluorescent Dyes

In order to image a sample using epi-fluorescence microscopy it has to be labeled with a fluorescent dye. Generally, the available dyes are divided into three classes: [32]: **(a)** Synthetic dyes, which are chemically engineered fluorophores which can typically bind specifically to a certain biomolecule, **(b)** Quantum dots, which are very bright and photostable but vast compared to most biomolecules and, **(c)** Autofluorescent proteins such as green fluorescent protein (GFP), which are occur naturally and are genetically encoded.

In 1992, Glazer *et al* reported the synthesis of new asymmetric cyanine dyes which specifically bind to DNA [34] and thus belong to the first class. The dye molecules consist of two groups of aromatic rings, the chromophores, which are linked by a bis-cationic linker. They bind to DNA by bis-intercalation of the aromatic groups between two neighboring base pairs. Due to their high quantum yields and the immense fluorescence enhancement upon binding to DNA (>1000 fold) these dyes became popular quickly and nowadays there is a wide range of intercalating DNA dyes available covering the whole range of visible light. One dye of this class, YOYO®-1 has been used throughout this thesis to stain DNA molecules. Its excitation and emission spectrum is shown in Figure 2.4 and its chemical structure is depicted in Figure 2.5.

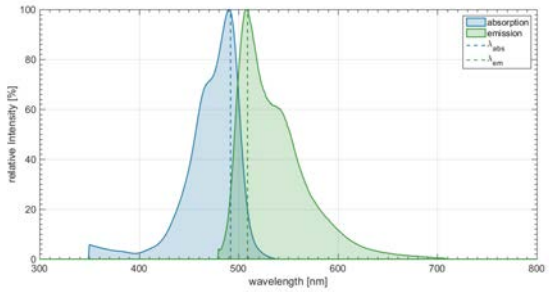

Figure 2.4: Excitation (blue) and emission (green) spectra for YOYO®-1 dye. The dashed lines indicate the excitation wavelength, λ_{ex} at 491 nm, and the emission wavelength, λ_{em} at 509 nm. Figure generated using data available in SpectraViewer by ThermoFisher Scientific [35].

As the YOYO®-1 dye binds to the DNA molecule by intercalation it alters the configuration of the DNA molecule and might therefore also affect some of its mechanical properties such as the contour and persistence length as well as the unwinding angle [36, 37, 38]. As nicely reviewed by Doyle *et al.*, [36], there are contradicting studies on the topic, which is most likely due to the very different experimental approaches as well as strongly varying buffer conditions and staining ratios. However, the most recent studies which made an effort to measure in chemical equilibrium seem to agree that the persistence length is unaffected by the staining, whereas the contour length increases by roughly 40% (for a molar staining ratio of 4:1) which corresponds to 0.5 nm per bound YOYO®-1 molecule [36, 37].

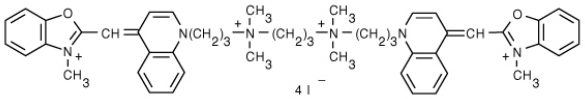

Figure 2.5: Chemical structure of the YOYO®-1 molecule [35].

2.3 Fluidics

Classical mechanics describe forces exerted on a particle's center of mass and the resulting motion. Since fluids are continuous media rather than discrete masses, their movement is better characterized by continuous mass and force density. The equation for the motion of fluids, the Navier-Stokes equation, is given by

$$\rho \left[\frac{d\mathbf{v}}{dt} + (\mathbf{v} \cdot \nabla)\, \mathbf{v} \right] = -\nabla p + \eta \nabla^2 \mathbf{v} + \mathbf{f}. \tag{2.7}$$

There, $\mathbf{v}$ is the flow velocity, ρ and η are the fluid's density and viscosity respectively, p is the pressure and $\mathbf{f}$ are external body forces. The left hand side of Equation 2.7 represents the inertial acceleration, consisting of the *local* acceleration term $\frac{d\mathbf{v}}{dt}$ and a non-linear term describing the *convective* acceleration, $(\mathbf{v} \cdot \nabla)\, \mathbf{v}$. The right hand side is an expression for the applied force density. Due to the non-linear term, the Navier-Stokes equation has no general analytical solution.

2.3.1 Fluidics on the microscale

Nevertheless, in regimes where inertial effects are negligible, the non-linear term in the Navier-Stokes equation can be neglected. To determine when this simplification holds, one can consult the Reynolds number, Re, which is defined as the ratio between inertial and viscous forces,

$$Re \equiv \frac{F_{\text{inertial}}}{F_{\text{viscous}}}. \tag{2.8}$$

With l and v being the characteristic length scale and velocity of the system respectively, the inertial and viscous forces can be defined as,

$$F_{\text{inertial}} = \eta l v, \tag{2.9}$$
$$F_{\text{viscous}} = \rho l^2 v^2, \tag{2.10}$$

which yields:

$$Re = \frac{F_{\text{inertial}}}{F_{\text{viscous}}} = \frac{\eta l v}{\rho l^2 v^2} = \frac{\eta}{\rho l v}. \tag{2.11}$$

In small scale systems such as microfluidic devices, typical length scales are in the μm range and flow rate are in the μm s^{-1} range. Thus, the Reynolds number is typically smaller than unity, $Re \ll 1$, which implies that viscous forces dominate over inertial effects and the flow profile is laminar. In contrast, fluids on the macro scale exhibit $Re \gg 1$, which yields turbulent flow conditions as we experience in every day life. The term laminar flow characterizes the parallel, undisturbed and non-mixing movement of a fluid, which is one of the essential prerequisites for Deterministic lateral displacement to function as explained in detail in Section 3.1.

2.3.2 Flow in a microchannel

There are many different mechanism for liquid transport in a microchannel. Four of the most important ones are: **(a)** Diffusion, which is further discussed in Section 2.3.3 and **(b)** capillary action, which are both passive transport mechanisms. And **(c)** electrokinetic movement as well as **(d)** pressure-driven flow, which are both active transport mechanisms as they require an actively supplied force to work. However, if a sample is contained in a liquid it has to be differentiated whether the above mechanisms move the sample or the surrounding liquid. While **(a)** and **(d)** cause the movement of both, **(b)** moves only the liquid and **(c)** moves only a charged sample.

In this work, pressure-driven flow was used for sample transport through a microchannel. There, a pressure gradient Δp is applied between the inlet and outlet of a channel. The flow velocity assumes a parabolic profile with the peak in the center of the channel. This can be derived using the no-slip boundary condition, which states that the velocity of the fluid is zero at the channel boundaries and is due to viscous drag from the channel boundaries [39].

Furthermore, in analogy to Ohm's law, the flow rate Φ through a channel can be described as,

$$\Phi = \frac{\Delta p}{R_h}. \tag{2.12}$$

However, for rectangular channels, as most frequently used in microfluidics, there is no analytical solution for the hydraulic resistance R_h. Instead, the following approximation is commonly used, [40],

$$R_h = \left[\frac{h^3 w}{12\eta L}\left(1 - 0.63\frac{h}{w}\right)\right]^{-1}, \tag{2.13}$$

where h, w and L are the height, width and length of the channel respectively.

2.3.3 Diffusion

Under laminar flow conditions diffusion is the only source of mixing. Diffusion is a passive mass transport mechanism which works against a concentration gradient and causes a particle flux $\mathbf{J}$ which can be described by Fick's law

$$\mathbf{J} = -D\nabla c, \tag{2.14}$$

where c is the concentration of the diffusing species and D is the diffusion coefficient. The Stokes-Einstein relation provides the diffusion coefficient for spherical particles,

$$D = \frac{k_B T}{6\pi\eta a}, \tag{2.15}$$

with k_B being the Boltzmann constant, T the absolute temperature, a the radius of the particle and η the dynamic viscosity. The mean square displacement $\langle r^2 \rangle$ of a diffusing particle in k dimensions is determined by

$$\left\langle r^2 \right\rangle = 2kDt. \tag{2.16}$$

This implies that the mean square movement of particles scales inversely with their radius. Thus, diffusion is more dominant on small scales. To determine the relevance of diffusion in a microfluidic system the Peclet number can be consulted. It is defined as the ratio of the diffusion and convection time

$$Pe \equiv \frac{\text{convection rate}}{\text{diffusion rate}} = \frac{\frac{L^2}{D}}{\frac{L}{v}} = \frac{Lv}{D}, \tag{2.17}$$

where L and v are the characteristic length and velocity respectively. In microfluidic systems the Peclet number is usually high, $10 < Pe < 10^5$, which suggests long mixing times [41].

A wider revision of the physics of fluidics on the microscale and the relevance of diffusion is provided by Austin *et. al.* [42].

Chapter 3

Experimental methods and details

This chapter will first give an introduction to the methodological approaches, comprising Deterministic Lateral Displacement (DLD) and nanofluidic devices, which both are direct applications of the before established theoretical concepts. Then, an introduction to the fabrication process in microfluidics will be provided. Finally, the experimental setup, procedure and details will be described.

3.1 Deterministic lateral displacement (DLD)

Deterministic Lateral Displacement (DLD) is a microfluidic particle separation method, which was first presented by Huang et. al in 2004 [6]. It is capable of deterministic, spatial separation of particles larger or smaller than a critical diameter, D_c. DLD devices consist of a periodic array of micrometer-sized obstacles, also referred to as posts, which are introduced into a microfluidic channel.

The geometry is designed such that the obstacles are contained in identical columns which are shifted vertically with respect to each other. Due to the laminar flow condition, this arrangement creates predictable, non-mixing streamlines. Figure 3.2a shows a sketch of a zoomed-in part of a DLD device indicating the arising streamlines.

The characteristics of a DLD device can be further defined by certain parameters. The center-to-center distance between two posts is denoted by λ and the edge-to-edge distance is denoted by d. The vertical shift between two columns can be written as $\Delta\lambda = \frac{\lambda}{n}$, which defines n as the periodicity of the array. The flow through the gap between two posts is thus divided into n lanes with equal flux $\frac{\Phi}{n}$. The described parameters are illustrated in Figure 3.1.

A device such as described above can be used to separate differently sized particles taking advantage

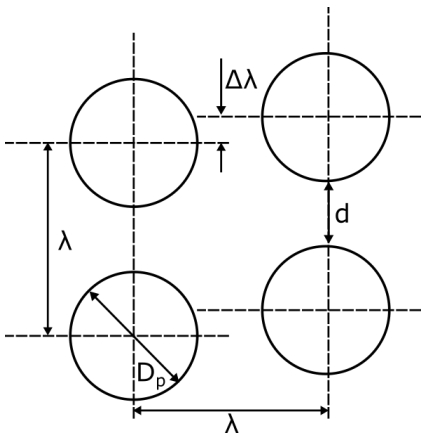

Figure 3.1: Sketch of a zoomed-in part of a DLD device indicating the parameters which define the post array. λ is the center-to-center distance between two posts, d is the post gap, D_p is the post diameter and $\Delta\lambda$ is the vertical shift between two columns of posts.

of the laminar streamlines. A particle whose center lies within the width of its current streamline, as the orange particle in Figure 3.2b, will be able to follow the same stream throughout the device. This motion is called *zigzag mode*. In contrast, a particle bigger than the width of its current streamline, as the purple particles in Figure 3.2b, will be deflected into the neighboring streamline upon each encounter with a post. Since this results in an overall spatial displacement, the motion is called *displacement mode* [41, 6]. Considering the described criterion for displacement it becomes clear that the width of the streamlines determines the critical diameter D_c, *i.e.*

$$D_c = \gamma \frac{d}{n}, \tag{3.1}$$

where γ the proportionality factor.

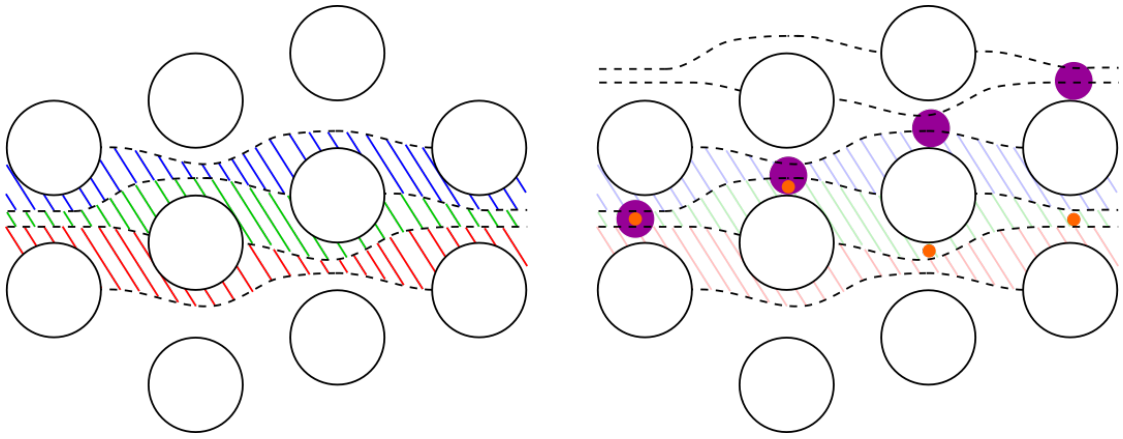

(a) Laminar streamlines. (b) Particle separation.

Figure 3.2: Sketch of a zoomed-in part of a DLD device illustrating the separation mechanism. The direction of flow is from left to right. (a) Illustration of emerging laminar streamlines. Cylinders are used as obstacles which define a periodic array. The periodicity of the shown array is $n = 3$. Thus, the flow divides into three non-mixing fluid streamlines (red, green, blue). (b) Illustration of separation mechanism. Differently sized particles are introduced into a DLD device. The orange particle is smaller than the width of its streamline and can thus pass through the device within the same streamline. The purple particle is bigger than the width of its streamline and is therefore deflected into the neighboring streamline at each encounter with a post.

Davis [43] has shown empirically that assuming a parabolic flow profile and cylindrical posts, the critical diameter in an can be approximated by,

$$D_c = 1.4 d \varepsilon^{0.48}, \tag{3.2}$$

where ε is the row shift fraction $\frac{\Delta\lambda}{\lambda}$ and d is the gap size. Furthermore, Wei *et al* [44] showed that Equation (3.2) is also applicable to differently shaped posts if expanded with a multiplicative factor α.

Generally, the posts in a DLD array can be of arbitrary geometrical shape. However, due to fabrication constraints, most devices use cylindrical posts with a circular cross section, as illustrated in Figure 3.1. Though, it has been shown that circular posts exhibit regions in close proximity to the post in which the flow velocity is zero such that particles tend to get trapped [41]. Since this effect is undesirable, other post shapes, like triangular, rectangular and streamlined (among others) have been implemented or simulated [44, 45, 46]. However, all DLD devices used throughout this thesis contain circular posts, whose diameter is denoted D_p, with $D_p = \lambda - d$.

3.1.1 Further aspects of DLD

When DLD was proposed, it was mainly intended for the separation of rigid spheres. However, already the original paper by Huang *et al.*, [6], provides a proof of principle that DLD is capable of separating DNA molecules by length using an electric field as driving force.

Furthermore, it has been shown that the principle of DLD can also be modified to separate particles based on shape and deformability [39]. For shape based separation, the device height can be used to control the alignment of the sample and therefore the effective size. This can for example be used to separate parasites from red blood cells [47]. Deformability-based separation can be achieved changing the shear stress on the particles by varying the flow rate. The effective size of highly deformable particles will decrease already at relatively low shear, *i.e.* flow rates and thus change their displacement behavior. Stiff particles on the other hand retain their shape and therefore also their trajectories through the device. This permits the separation of similarly sized particles with different deformability [48].

DLD devices can also be used for multiple separation. Usually, a DLD device has only one critical diameter, D_c, throughout the whole device and can therefore only provide bi-modal separation. It is however possible to fabricate devices in which the critical diameter changes for different sections of the device permitting multimodal separation. These devices require typically a precisely optimized outlet design to collect all separated fractions individually.

3.1.2 Diffusion in DLD

As explained in Section 2.3.3, diffusion is an inevitable process at the microscale and therefore needs to be taken into consideration when dealing with any microfluidic particle separation method. As opposed to most other passive particle separation methods such as the H-filter [42] or size exclusion chromatography [49], DLD does not depend on diffusion. On the contrary, diffusion is an undesirable effect which typically worsens separation quality since it leads to mixing of the laminar streamlines. Especially if particles are significantly smaller than μm-sized, the stream broadening due to diffusion might be larger than the spatial separation achieved by DLD. Therefore, device and experiment have to be designed carefully, ensuring that Reynolds and Peclet numbers are in the correct regime.

3.2 Fabrication of microfluidic devices

During the last decade, a standard method for the fabrication of microfluidic devices emerged. Though, every particular fabrication process has to be adjusted to the specific device and its application. The standard method comprises steps from UV and soft lithography. Typically, a silicon wafer is patterned by UV lithography with a microstructure, which had beforehand been designed on the computer. Solely the fabrication steps involving soft lithography were carried out in the course of this thesis and are therefore described in more detail.

3.2.1 Polydimethylsiloxane (PDMS)

Polydimethylsiloxane (PDMS) is a silicon-based hydrophobic polymer which is widely used for the soft lithographic fabrication of microfluidic devices [50, 51]. It consists of an inorganic siloxane backbone to which organic methyl groups are bound. PDMS is described by the chemical formula $CH_3[Si(CH_3)_2O]_nSi(CH_3)_3$, where $[Si(CH_3)_2O]$ is a n times repeating unit [52].
The common usage of PDMS within the microfluidic community is due to its many advantageous properties. Its elastic properties make it possible to mold PDMS into quasi-three-dimensional structures which can easily be pulled off from a treated silicon mask. Furthermore, PDMS does not swell in humidity, is permeable for gases and thermally stable up to high temperatures. However, its most convenient property is that it is optically transparent down to 300 nm which makes it suitable for experiments using epi-fluorescence microscopy [50].

3.2.2 Soft Lithography

The term soft lithography describes the process of replicating a structure from a mould into an elastomeric material [50]. Here, a commercially available PDMS kit is used as elastomeric material. First, PDMS is mixed with the curing agent in a ratio 10:1

(a) The mould, a silicon wafer fabricated by UV lithography, contains the imprint for microfluidic devices.

(b) A mixture of PDMS and curing agent (10:1) is poured onto the wafer in a thin layer.

(c) After curing for one hour at 80 °C, the PDMS can be peeled off the wafer. The PDMS piece is a negative imprint of the mould.

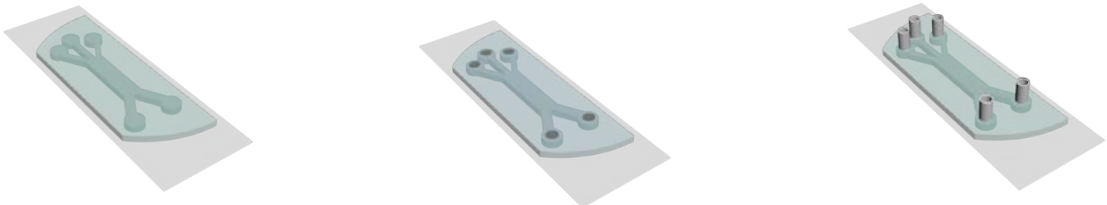

(d) The desired device is cropped from the PDMS piece and put onto a glass slide.

(e) Holes for the inlets and outlets are punched into the PDMS and biith, glass slide and PDMS piece are plasma treated.

(f) After the bonding of glass slide and PDMS, small plastic tubes are glued onto the device which serve as inlet and outlet reservoirs.

Figure 3.3: Illustration of the soft lithography fabrication process for microfluidic devices.

and poured onto the patterned silicon wafer. The PDMS is cured in the oven at 80 °C for one hour and can then gently be removed from the silicon wafer and shows an inverse imprint of the micro-structure on the wafer. The PDMS piece is cut to size and holes for inlets and outlets are punched. Plasma-activated bonding is used to seal a glass slide and the PDMS piece to create micro-channels. Finally, plastic tubes which serve as reservoirs are glued on top of the inlet and outlet holes. An illustration of the listed steps is shown in Figure 3.3 and a detailed protocol is given in Appendix A.1.

3.3 Nanofluidic devices for length measurements

As explained previously, confined DNA molecules stretch out along the axis of confinement and the relative extension is proportional to their contour length. Recently, nanofluidic devices have been developed which confine DNA molecules in nanochannels for direct observation on the single molecule level and thereby allowing to optically determine the length of a DNA molecule [18, 53].

A device consists of a silicon chip with a design as sketched in Figure 3.4 with a glass cover. The chip is fabricated using standard semiconductor fabrication techniques. The nanochannels which are the central component of the device are at top and bottom connected to a U-shaped microchannel which are in turn linked to a reservoir on each side. Typically, all reservoirs are pressure controlled, the DNA sample is inserted into one of the reservoirs and moderate pressure (up to 1 bar) is applied to transport the sample to the nanochannel section. Entering the nanochannels constitutes a substantial entropic barrier for a DNA molecule [8, 54]. This can be overcome by applying a pressure pulse. As soon as DNA has entered the nanochannels single molecules can be imaged using epi-fluorescence microscopy.

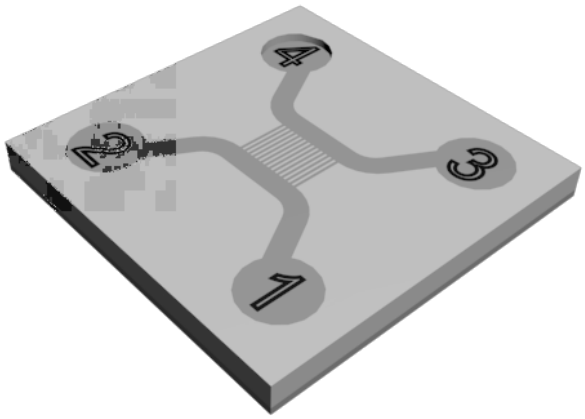

Figure 3.4: Sketch of a nanochannel device. The nanochannels connect the two U-shaped microchannels which are linked to reservoirs on each side.

3.4 DNA separation experiments

As explained previously, free DNA adopts the shape of a random coil whose radius depends on the length of the DNA molecule. Therefore, deterministic lateral displacement is a reasonable approach to separate DNA molecules by length. For this thesis, three different DNA samples were tested in two different DLD devices to determine whether this method allows length-based separation of DNA molecules.

The devices used were not specifically designed for DNA separation experiments. Instead, devices with appropriate parameters for which a mold was readily available were used. The parameters of the used devices are presented in Table 3.1. During the device and

manufacturing process each device is assigned a number, #6 and #10 for the relevant devices. To avoid confusion, this naming will be maintained throughout the thesis. Both devices have a very similar design consisting of two inlets with channels leading into a pillar array and five outlets. A sketch of device #10 is given in Figure 3.6.

Table 3.1: Overview of used DLD devices and parameters.

	#10	#6
D_c [μm]	0.64	0.75
d [μm]	3	3
n	50	38
D_p [μm]	15	15

3.4.1 DNA samples

Three different types of DNA, referred to as Ladder, Lambda and T4, were used as sample for the conducted experiments. An overview of the relevant parameters is given in Table 3.2.

Ladder DNA is a set of DNA fragments with well-defined length distribution typically used as size or molecular weight marker in the context of gel-electrophoresis. The here used Ladder DNA consists of fragments from 250 bp to 10 kbp and was purchased as GeneRuler 1kb DNA Ladder from Thermo Scientific. The stock concentration is 0.5 μg/μl.

Lambda DNA is double stranded, viral DNA isolated from bacteriophage lambda. It consists of 48.5 kbp with a short, single-stranded, complementary overhang, so called *sticky ends*. The employed sample of Lambda DNA was purchased form New England BioLabs. The stock concentration is 0.5 μg/μl.

T4 DNA is double stranded viral DNA isolated from bacteriophage T4 species. It consists of 165.6 kbp. The sample was purchased as T4 GT7 DNA from Wako Chemicals. The stock concentration is 0.32 μg/μl.

Table 3.2: Overview of DNA samples including number of base pairs N, contour length L and Flory radius R_F, assuming the effective width to be 5 nm. The values for L and R_F take to elongation due to staining with YOYO®-1 (ratio 10:1) into account.

	$\text{Ladder}_{\text{min}}$	$\text{Ladder}_{\text{max}}$	Lambda	T4
N [kbp]	0.25	10	48.5	165.6
L [μm]	0.10	3.9	18.9	64.6
R_F [μm]	0.06	0.50	1.29	2.69

3.4.2 Sample preparation

Sample preparation of the DNA included mainly the staining of the DNA with the fluorescent dye YOYO®-1 and dilution in the buffer solution.

The staining of the DNA was simply performed by mixing the sample and the dye in a molar ratio 10:1 in an Eppendorf tube. The staining protocol was chosen such that the volume ratio of sample and dye was 1:1. The exact concentrations and volumes for all DNA types are given in Appendix A.2.

After staining, the sample can be imaged on a glass slide to determine a suitable dilution factor. The buffer solution which was used for dilution during all DNA separation experiments was a 0.5x TAE buffer, containing 1% BME. TAE buffer solution is commonly used in molecular biology when handling DNA. TAE contains a mixture of tris-base, acetic acid and ethylenediaminetetraacetic acid (EDTA) of which the latter functions as a chelating agent preventing the degradation of DNA by enzymes. BME, also β-mercaptoethanol, is a sulfite containing chemical which is often added to the buffer in fluorescence experiments since it scavenges radicals and thus enhances the photostability of the dye [55].

3.4.3 Setup

A picture of the setup for a DNA separation experiment is shown in Figure 3.5 (*left*). The core element of the setup is an epi-fluorescence microscope, which is assembled just as sketched in Figure 2.3. The microscope is furthermore equipped with a white lamp such that it can be used for regular and fluorescent imaging. For imaging DNA separation experiments, a 20x air objective with NA = 0.45 was used. Moreover, the setup contains a microfluidic pressure control system, called Fluigent, which is used to induce pressure-driven flow inside the device. The Fluigent could provide pressure up to 77 mbar in up to four different channels. Typically, the microfluidic device is mounted on the microscope stage and two pressure tubes from the Fluigent are connected to the inlet tubes as shown in Figure 3.5 (*right*).

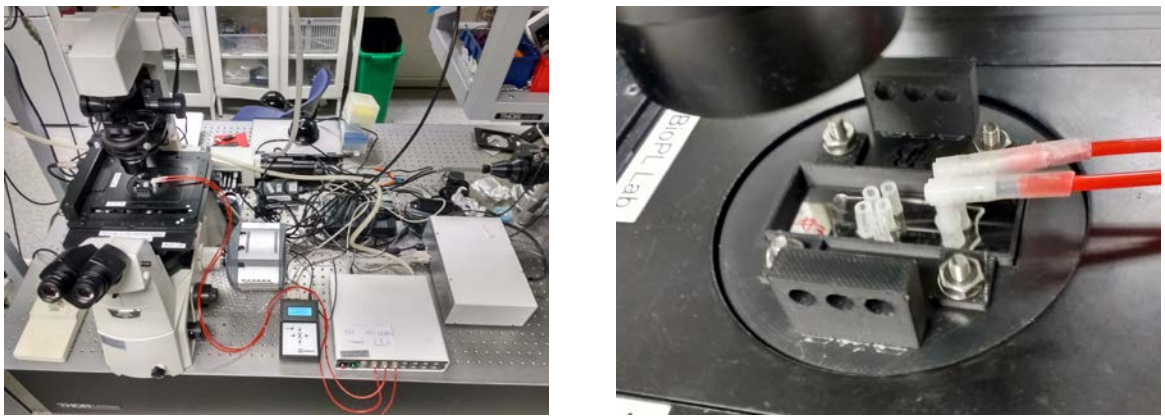

Figure 3.5: Images of the setup for DNA separation experiments (*left*) giving an overview of the epi-fluorescence microscope and the pressure control system and (*right*) a close-up of a mounted DLD device with pressure tubes from the Fluigent connected to the inlets.

3.4.4 Conducting a DNA separation experiment

Prior to running a DNA separation experiment, all preparatory steps, which involve **(a)** the assembly of the optical setup including the insertion of the correct filter (FITC) and objective (20x air), **(b)** the setup of the microfluidic flow control system, the Fluigent, **(c)** the fabrication of a microfluidic device as described in Section A.1, **(d)** the staining of the DNA sample with the fluorescent YOYO®-1 dye as outlined in Section A.2 and **(e)** the dilution in a 0.5x TAE, 1% BME buffer solution by a factor 500 from stock need to be completed.

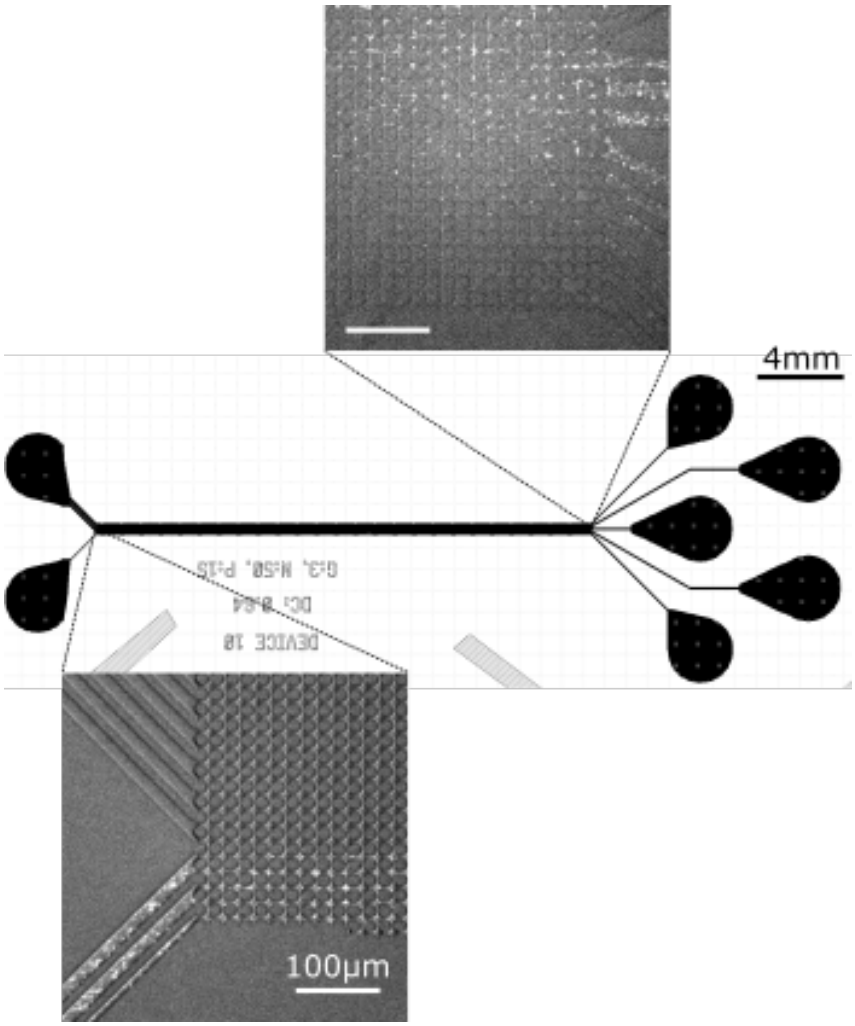

Figure 3.6: Sketch of a DLD device #10 as used for DNA separation experiments. Inlets are on the left side, outlets are on the right side and flow goes from left to right. The sample is introduced at the lower inlet and enters the device as shown in the bottom inset. Inlet (*right/bottom*) and outlet (*left/top*) fluorescence images of a typical DNA separation experiment. The insets are images of device #10 loaded with Lambda DNA at an applied pressure of 10 mbar.

Then, the microfluidic device is flushed with 0.5x TAE, 1% BME buffer solution. If necessary, air bubbles are removed. Next, the DNA sample is inserted into the sample inlet and the FLuigent is connected to apply pressure and transport the sample through the device. Typical images of DNA at the inlet and outlet are shown in Figure 3.6. Movies with 800 frames are taken at the outlet to record the result. A detailed protocol for conducting a DNA separation experiment is given in Appendix A.3.

Typically, during one experiment, one DNA sample is run at varying applied pressures. At an early stage, experiments were carried out at 10 mbar, 40 mbar and 77 mbar whereas later experiments were carried out at 10 mbar, 20 mbar, 30 mbar, 40 mbar, 50 mbar, 60 mbar, 70 mbar and 77 mbar to be able to better investigate the pressure dependence.

3.4.5 Problems with DNA separation experiments

Here, a brief discussion of the most common challenges which arose when conducting the experiments is given.
Firstly, it can happen that despite the plasma treatment, the bonding between glass and PDMS fails partly. This leads to leakage as soon as the sample is loaded and pressure is applied. A leaking device is completely nonfunctional and has to be disposed.
Another common issue is air bubbles inside the device or at the inlets or outlets. This is usually due to lapses during the manufacturing process or due to drying out during prolonged storage times. Usually, air bubbles can be removed using the *purge* function of the Fluigent, which provides a high pressure (500 mbar) on one inlet channel and dissolves air bubbles into the buffer. If the air bubbles cannot be removed, the device has to be disposed since their presence does not allow controlled pressure conditions.
The last issue to be mentioned is that the device is designed such that the outlet channels are of different lengths as shown in Figure 3.6. From Equation 2.13, it is apparent, that longer channels exhibit higher hydraulic resistance than shorter channels. Therefore, the flow velocity in outlet channels 2 and 4 were slow relative to the other channels and DNA molecules tended to slip into adjacent channels with lower resistance. This particular problem is taken care of by the image analysis as described in Section 4.2.

3.5 Nanochannel experiments

As a complement to the DNA separation experiments, this thesis includes nanochannel experiments. As described in Section 3.3, nanochannel devices can be used to measure the length of a DNA molecule. Since size, which implies length regarding DNA molecules, is the critical parameter in the separation experiments using DLD devices, it is essential to know the precise length distribution of the investigated sample. Therefore, nanochannel experiments were performed to determine the length distributions of the Lambda and T4 DNA sample. The knowledge of the length distribution can then serve as frame of reference for the DNA separation experiments. The samples were prepared as already described for the DNA separation experiments.

3.5.1 Setup

The optical setup was equivalent to the setup for the DNA separation experiments as shown in Figure 3.5 (*left*). To have adequate resolution on the single molecule level, a 60x oil immersion objective with NA = 1.40 was used for image acquisition.

A sketch of the chip design is shown in Figure 3.4. The dimensions of the nanochannels are 100x150 nm. Pressure-driven flow is used for sample transport within the device.

However, due to the device design, the requirements for the pressure control system are more complicated. Therefore, a custom-made pressure control panel, which allows control over four channnels up to 2 bar and can provide pressure pulses was used. A picture of the mounted chip and the pressure control system is presented in Figure 3.7.

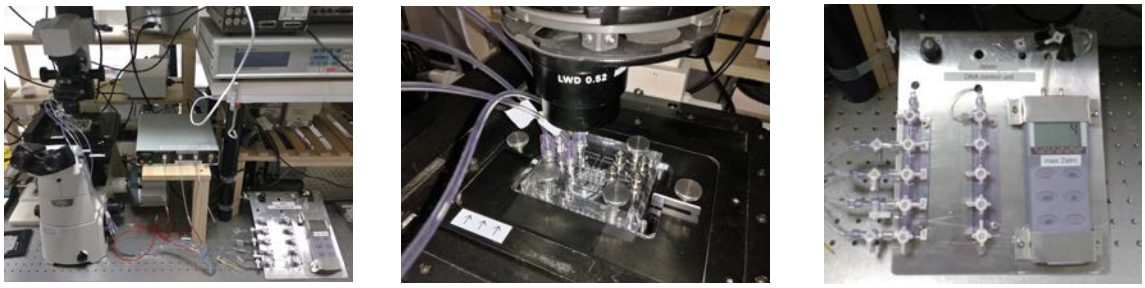

Figure 3.7: Images of the nanochannel setup featuring an overview image (*left*), the chip mounted on the microscope stage (*center*) and the pressure control system (*right*).

3.5.2 Conducting a nanochannel experiment

Before running a nanochannel experiment, all preparatory steps, which involve **(a)** the assembly of the optical setup including the insertion of the correct filters (FITC) and objective (60x oil), **(b)** the setup of pressure control unit, which is shown in Figure 3.7, **(c)** the staining of the DNA sample with the fluorescent YOYO®-1 dye as outlined in Appendix A.2 and **(d)** the dilution in a 0.5x TAE buffer solution by a factor 2000 from stock need to be completed.

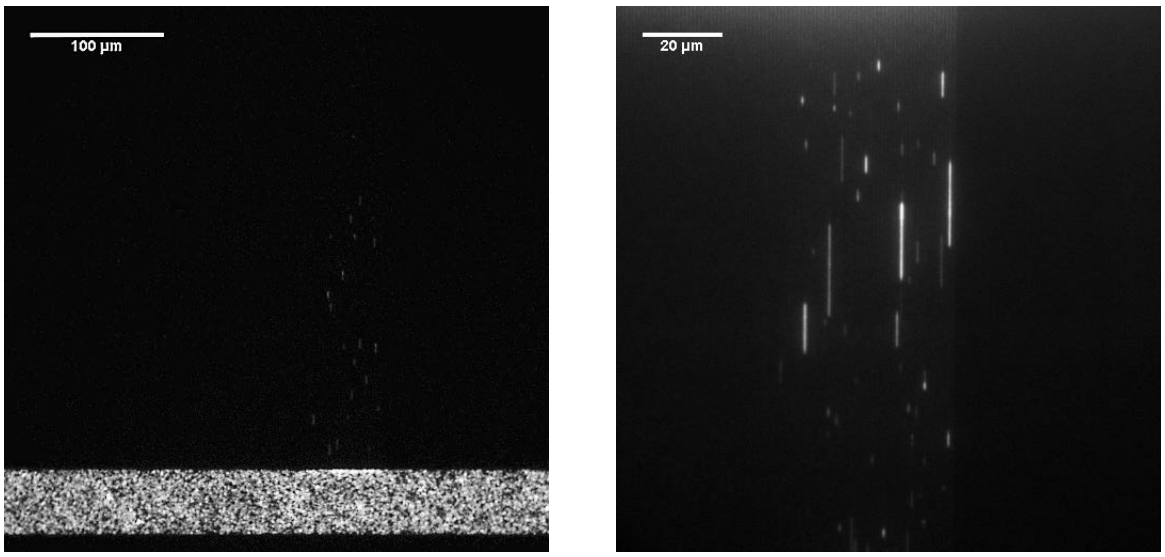

Figure 3.8: Fluorescence images of DNA molecules in the nanochannel device. (*Left*) Image (20x magnification) of the nanochannel device showing Lambda DNA molecules mostly in the microchannel (bottom) with a considerably higher concentration at the entry to the nanochannels. Also, some molecules which have already entered the nanochannels are discernible. (*Right*) Image (60x magnification) showing T4 DNA molecules confined and stretched in nanochannels.

When the preparations are finished, the nanochannel device is flushed with 0.5x TAE buffer solution. Then, the DNA sample is inserted into one of the reservoirs and flushed

through the adjacent microchannel. The pressure is adjusted such that DNA molecules are assembled at the entry to the nanochannels which they cannot enter due to entropic hindrance. Only upon the application of a pressure pulse can the DNA molecules enter the nanochannels in which they are confined and thus stretched out. Figure 3.8 shows the bordering region between the micro- and nanochannel directly after the pressure pulse. Subsequently, the pressure is turned off which causes the confined DNA molecules to become stationary and equilibrate. This is shown in Figure 3.8 (*right*). Typically, movies with 100 frames are taken which are later used to deduce the lengths of the DNA molecules. A detailed protocol for conducting a nanochannel experiment is given in Appendix A.4.

Chapter 4

Image analysis

In order to extract quantitative results from the acquired data, image analysis has to be performed. For this purpose, both MATLAB and ImageJ were used. In the following, the image analysis methods and algorithms which were applied to the raw data will be described in chronological order as an image was processed. However, only the most important steps are described in more detail but all code files are available in Appendices B and C for the MATLAB code and ImageJ macros respectively.

4.1 Background subtraction

Typically, the first step in image analysis, is background subtraction. To compute a background image for every image stack, the MATLAB function *CalculatingQuantile* was written. Based on an image stack with N frames, *CalculatingQuantile* finds the intensity distribution for every pixel in an image and reads out the intensity at the provided quantile value q. This intensity value is then assigned to the corresponding pixel in the background image. Since the computation proved to be rather heavy, the intensity distribution was calculated from a randomly selected sub-stack with nN elements. Therefore, the quantile is effectively given by qn.

Once the background image had been calculated, it was subtracted from the corresponding raw image stack, which was then averaged. Figure 4.1 provides example images of the background subtraction process. Subfigures (a) and (c) show the same image stack before and after background subtraction with the corresponding background image which is shown in (b).

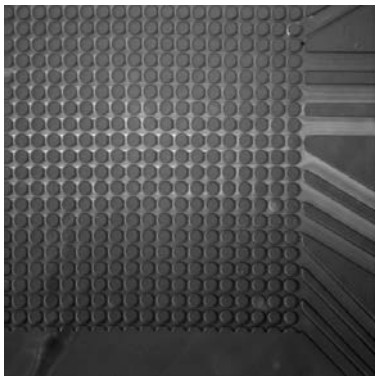

(a) Average over raw image stack.

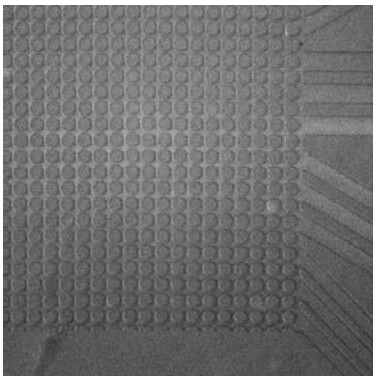

(b) Calculated background image.

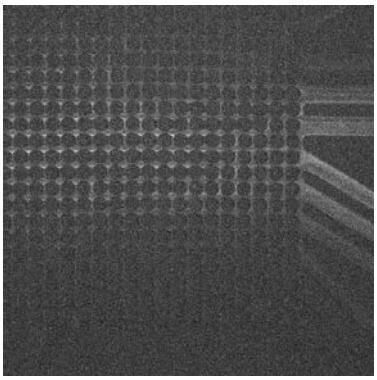

(c) Average over background subtracted image stack.

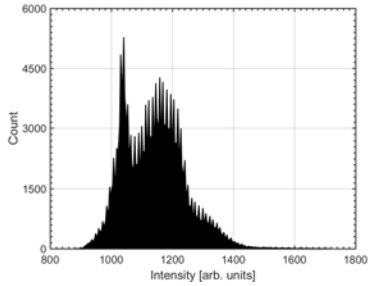

(d) Intensity histogram of raw image stack average.

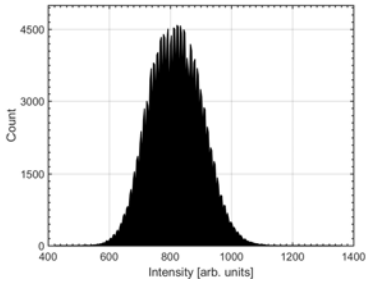

(e) Intensity histogram of computed background.

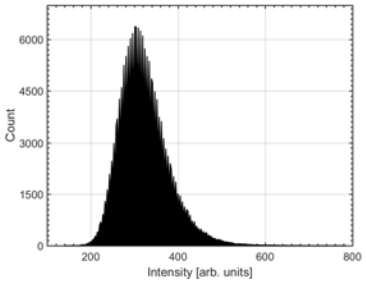

(f) Intensity histogram of background subtracted image stack.

Figure 4.1: Illustration of background calculation and subtraction. The average over a raw image stack (a) and the corresponding intensity histogram (d) are shown. *CalculatingQuantile*, with $q = 0.03$ and $n = 0.25$, is used to compute the background of (a). The resulting background image and its intensity histogram are shown in (b) and (e) respectively. Then, the background (b) is subtracted from the raw data (a) which results in the background subtracted image (c) with the intensity histogram (f). While the unprocessed image (a) clearly shows features of the device, the processed image (c) shows purely the fluorescent image.

4.2 Intensity profile

Since a 20x magnification objective was used for acquiring the images, the field of view was not big enough to record the whole outlet of the device at once. Instead, one stack for bottom and top of the device were acquired. To quantify the amount of DNA at the outlet, a reliable method to plot the intensity vertically along the device at a reproducible position had to be developed. In order to avoid the outlet effects influencing the measurement results it is desirable to plot the intensity several rows of posts before the actual outlet. To do so, a MATLAB script *ImageAnalysisFinal*, available in detail in Appendix B.4 was implemented. It includes the following components:

1. Rotating and cutting top and bottom images according a to passed rotation angle. This is done by the minor function *ImageRotationFunc*, Appendix B.3.

2. Identifying the column of the device boundary, which means the column where the post array ends and the outlet begin. The approach is to compute a moving standard deviation of the intensity in y-direction. The maxima of the moving standard

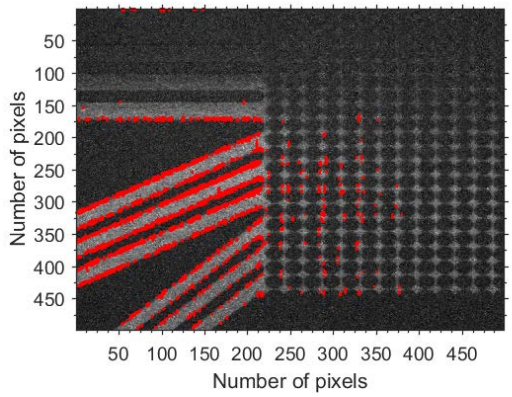

Figure 4.2: Fluorescence image of the bottom part of the device outlet. The red dots indicate the positions where the intensity showed the largest moving standard deviation in y-direction.

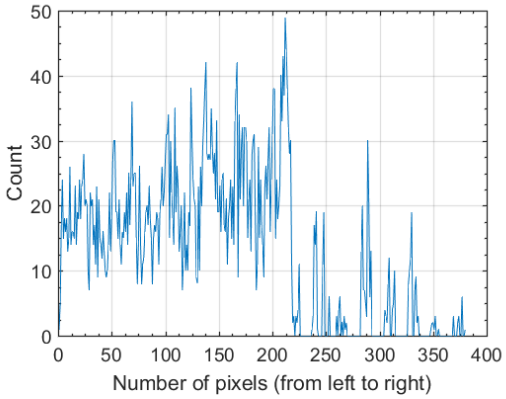

Figure 4.3: Histogram over x-occurrences of maxima in Figure 4.2.

deviation arise where the contrast is largest, i.e. at the edges of the outlet channels and posts, as illustrated in Figure 4.2. By creating a histogram of the maxima's x-values and finding the most prominent dip, as presented in Figures 4.3 and 4.4 respectively, one can get an estimate for the location of the device boundary. The position of this guess is indicated with a blue line in Figure 4.5.

3. Searching a defined neighborhood around the estimate and identifying the column with the highest average intensity is assumed to yield the boundary column, since it is the only column without interruption by channels or posts. The position of the device boundary is marked with an orange line in Figure 4.5.

4. In order to plot the intensity a certain number of rows before the outlet boundary one has to know the width of one post. This can be found using the MATLAB script *FindingPostSize*, presented in Appendix B.2, which computes a spatial correlation function to determine periodicity in the post array. Knowing the post size, the intensity at a fixed point before the outlet can be read out. Here, the intensity was plotted seven rows before the device boundary, as shown by the yellow line in Figure 4.5.

5. Writing the intensity along this column into a separate variable.

The algorithm as described above was run individually for each top and bottom image. To create an intensity profile along the whole device, corresponding images and intensity profiles of the same pressure had to be merged vertically. The built-in correlation function in MATLAB was used to find the rows with highest correlation. An example of a merged image is shown in Figure 4.6. Since only a vertical fuse is desired, inaccurate merges in x-direction are irrelevant. Having obtained the coinciding row numbers of two images, the intensity profiles can be merged accordingly. As seen in Figure 4.6, the merged images usually have a slightly different background level. To correct for this, the mean intensity of the overlapping area is adjusted. This yields a final intensity profile along the whole device seven rows before the device boundary as shown in Figure 4.7.

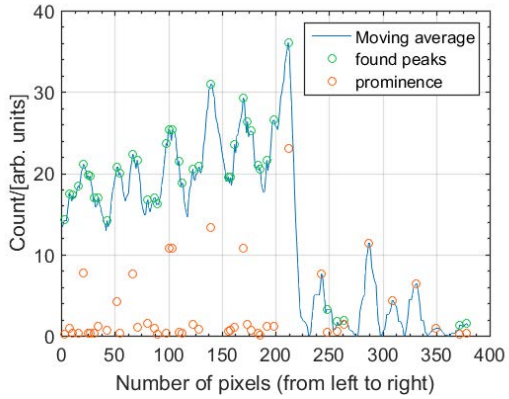

Figure 4.4: Plot of the moving average over the histogram of x-occurences, Figure 4.3. The green circles indicate the position of detected maxima in the moving average. The orange circles indicate the prominence of the detected peaks.

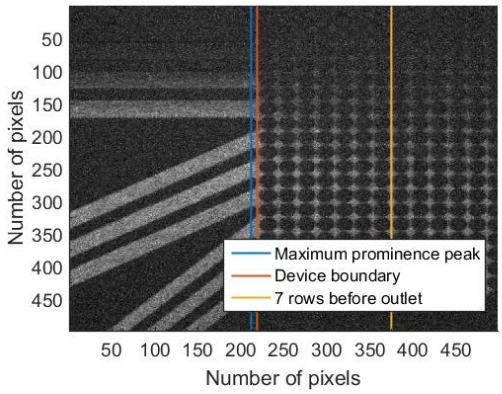

Figure 4.5: Fluorescence image of the bottom part of the device with lines indicating the maximum prominence peak (blue), the device boundary (orange) and the seventh row of posts before the device boundary. The position of the lines was calculated using the described algorithm.

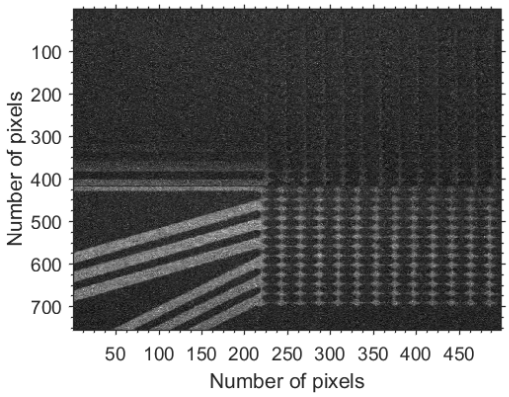

Figure 4.6: Top and bottom images of the device merged. The merge serves only the determination of the y-coordinate. An inaccurate merge in x-direction is irrelevant.

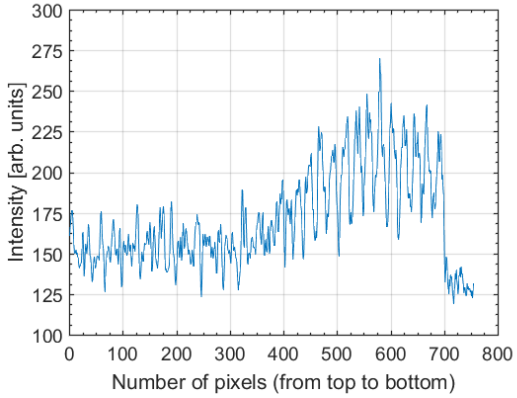

Figure 4.7: Intensity plot across the device at the position marked with yellow in Figure 4.5. The periodic dips in the intensity profile correspond to the positions of the posts in the DLD array.

The *IntensityAnalysisFinal* script is written such that it recognizes all *tif*-files in one folder and can perform the above described analysis on an entire data set, assuming that top and bottom images are labeled with even and odd numbers respectively. However, in rare cases, certain parameters are not applicable to the complete data set but need to be altered, i.e. the script had to be executed repeatedly for different pressures.

4.3 Cumulative function

Up to this point, the performed analysis yields an individual intensity profile for each device, sample and pressure combination. In order to comparatively analyze the data, different profiles have to be plotted into the same graph. This is done in Figure 4.8 which shows the intensity profiles of one data set, in this case Lambda DNA in device #10. It

is apparent, that the background is different for every curve.

To make the curves for different pressures comparable, each one is fitted to the sum of a Gaussian and a linear function,

$$f_{\text{fit}}(x) \;=\; a \exp\left(-\frac{(x-b)^2}{2c^2}\right) + dx + e. \tag{4.1}$$

It is assumed that the signal is Gaussian shaped and the background is linear, which is most likely due to nonuniform illumination. Therefore, subtracting the linear part of the fit from the data yields a background adjustment as shown in Figure 4.9.

For better visualization, the subsequently presented results will be shown in a cumulative plot as in Figure 4.10. In the graph, the integral of the relative intensity is plotted across the length of the device, *i.e.* each intensity profile from Figure 4.9 is normalized and the individual values are added along the x-axis.

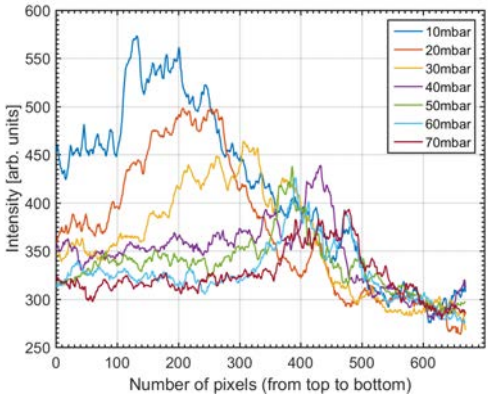

Figure 4.8: Intensity profile of Lambda DNA at different pressures in device #10.

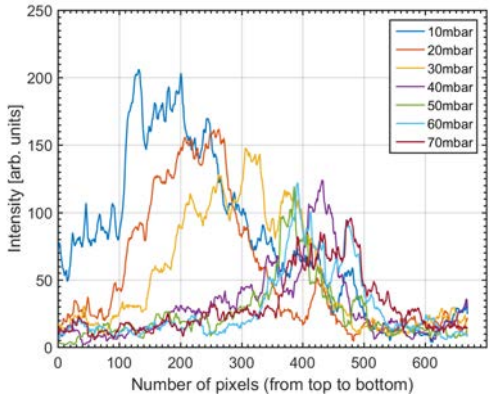

Figure 4.9: Background subtracted intensity profile of Lambda DNA at different pressures in device #10. The background subtraction is performed by fitting the data to Equation 4.1 and subtracting the linear part.

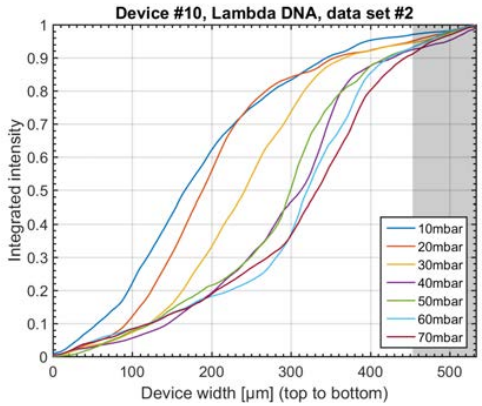

Figure 4.10: Example of cumulative plot. The relative integrated intensity (integrated and normalized from Figure 4.9) is plotted across the width of the device.

Chapter 5

Results and Discussion

In this chapter, the experimental results will be presented and discussed. Firstly, an experiment proving the linearity of applied pressure and flow velocity will be presented. This will be followed by a thorough analysis of the DNA separation experiments and the results of the length measurements in the nanofluidic device. Finally, the presented results will be discussed and the most important aspects will be summarized.

5.1 Pressure-velocity dependence

As described previously, all DNA separation experiments in DLD devices were carried out using the Fluigent to induce pressure-driven flow. Therefore, the applied pressure was the parameter which was altered to change the flow rate. Accordingly, the results presented in the following Section 5.2, are in dependence of the applied pressure. However, for the interpretation of the results the change in flow velocity is decisive. Thus, it was necessary to determine the relationship between the applied pressure and the flow rate.

To do so, a series of measurements with 0.51 μm polystyrene beads in device #10 was taken. The pressure was increased from 5 mbar to 30 mbar in 5 mbar increments. At each step, 2000 frames with illumination time 50 ms were acquired. For the analysis, ImageJ was used to generate images of the maximum intensity of a few subsequent frames. The macro which was written for this purpose is available in Appendix C.1. One of these generated images is presented in Figure 5.1. Clearly, single bead tracks can be discerned. Measuring the length of these tracks, taking into account the magnification and the illumination time, the flow velocity could be determined. For each pressure, approximately 200 particle tracks were measured. A plot of the average velocity versus the applied pressure is shown in Figure 5.2. The data can be fitted well with a linear fit. This means, it is justified to plot the results against a linear pressure axis, which corresponds to a linear velocity axis with unknown units.

To explain the large standard deviation, one has to consider that the beads are smaller than the critical size of the device. Thus, they move in *zigzag* mode, which means they go vertically between two posts every N^{th} post just as the particle marked with blue in Figure 5.1. If a particle just performed this actual *zigzag* movement it travels fast through the device, almost free of interactions with the posts. On the other hand, a particle which

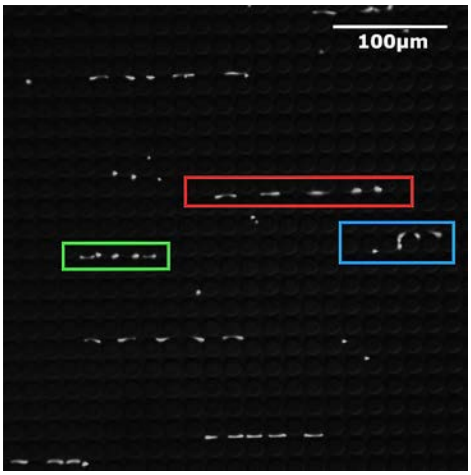

Figure 5.1: Image from MAX intensity over 5 frames with ImageJ. Particles are in different stages of the *zigzag* mode. Blue: Performing the *zigzag* movement, red: Fastest phase, shortly after performing the *zigzag* movement basically undisturbed by the posts, and green: slowest phase, when bumping into posts shortly before performing the *zigzag* movement.

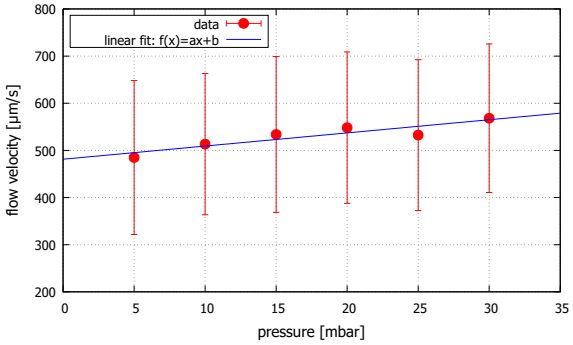

Figure 5.2: Plot of flow velocity versus applied pressure for 0.51 μm polystyrene beads. Each data point is the average velocity determined by measuring approximately 200 particle tracks. The errorbars indicate the standard deviation. The blue line depicts a linear fit to the data.

is just approaching a vertical transition moves only slowly due to increasing collisions with the posts. In Figure 5.1 an example for a fast track is marked with red and a slow track with green.

5.2 DNA separation results

As it is also natural in the course of an experiment, the first step is to look at the qualitative results to check whether the chosen approach yields interesting results. Figures 5.3 and 5.4 show the outlet of device #10 at 10 mbar and 77 mbar applied pressure respectively, where in each (a) displays the device without sample, (b) with Ladder DNA, (c) with Lambda DNA and (d) with T4 DNA, where (b)-(d) are fluorescent images. The sample is introduced in a four post wide stream on the right side of the device as shown in Figure 3.6.

Considering Figures 5.3 and 5.4 one can first and foremost see that that the behavior of Ladder DNA greatly differs from the behavior of Lambda and T4 DNA. Ladder DNA travels straight through the device and exits the device mainly through the two bottom outlets whereas Lambda and T4 DNA are subject to lateral displacement and exit mainly through the two top outlets. Secondly, it is evident all three types of DNA show a notable broadening of the sample stream compared to the four post wide stream at the inlet.

The lateral displacement of the sample stream which can be observed for Lambda and T4 DNA, but not for Ladder DNA, is caused by the displacement mechanism of DLD. This indicates, that the coil of Lambda and T4 DNA are exceeding the critical diameter of device #10. Though, comparing (c) and (d) of Figures 5.3 and 5.4, it seems that higher pressure has an effect on the displacement achieved by DLD. In the ideal model featuring rigid spheres, the separation mechanism of DLD is velocity-, *i.e.* pressure-independent,

but since DNA is neither rigid nor spherical other effects such as shear forces play a role.

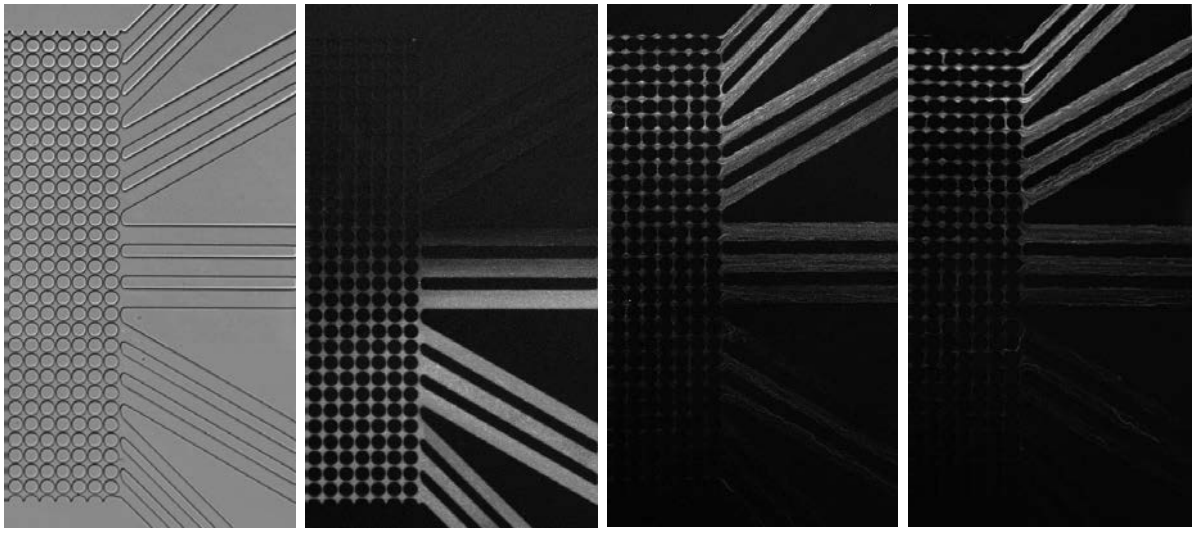

(a) Outlet device #10 (b) Ladder DNA (c) Lambda DNA (d) T4 DNA

Figure 5.3: Ladder, Lambda and T4 at outlet of device #10 using 10 mbar pressure. The direction of flow is from left to right. The image displays the maximum intensity of a stack with 800 frames.

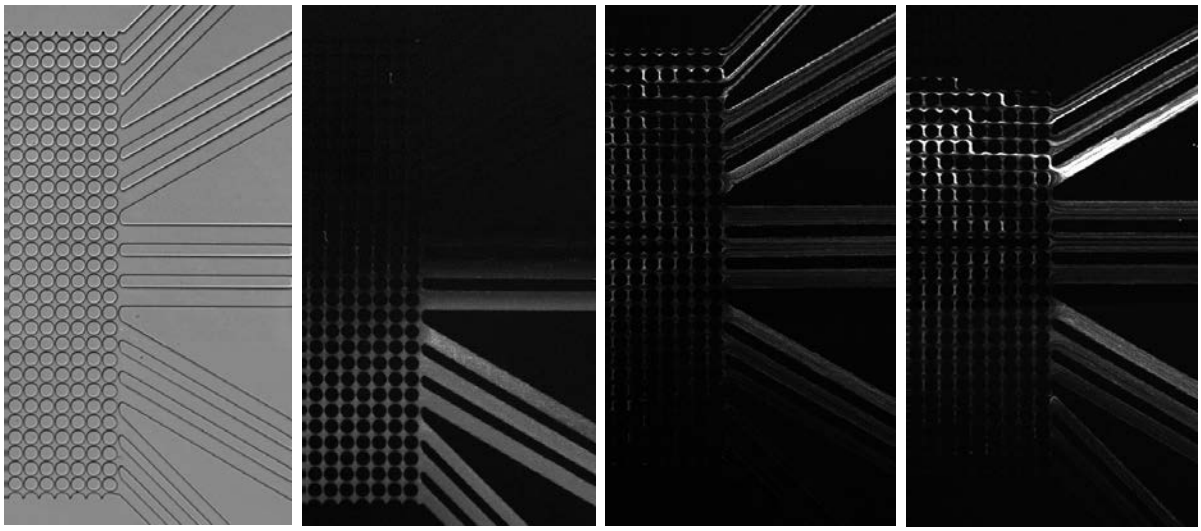

(a) Outlet device #10 (b) Ladder DNA (c) Lambda DNA (d) T4 DNA

Figure 5.4: Ladder, Lambda and T4 at outlet of device #10 using 77 mbar pressure. The direction of flow is from left to right. The image displays the maximum intensity of a stack with 800 frames.

Summarizing this first qualitative investigation, it is apparent that DLD is a promising approach for length based DNA separation and is therefore further investigated. Especially owing to the behavior of long DNA at high pressure, it can be suspected that the separation mechanism is not quite as straightforward as predicted by the DLD theory. This might be due to the influence of thermal motion, diffusion and the complex behavior of DNA under hydrodynamic shear forces.

5.2.1 Pressure dependent results

On the whole, twelve data sets were acquired, two for each device and DNA sample combination. In this section, each data set shall be presented individually, which at the same time provides a pressure dependent analysis.

The following plots show the integrated intensity of the DNA over the width of the device outlet in pixels. The pixel number zero corresponds to the top of a device and increases downwards. Note, that the sample stream enters a device at the bottom and is roughly 100 pixels wide upon entry. This corresponds approximately to the region from pixel number 550 upwards in the following plots.

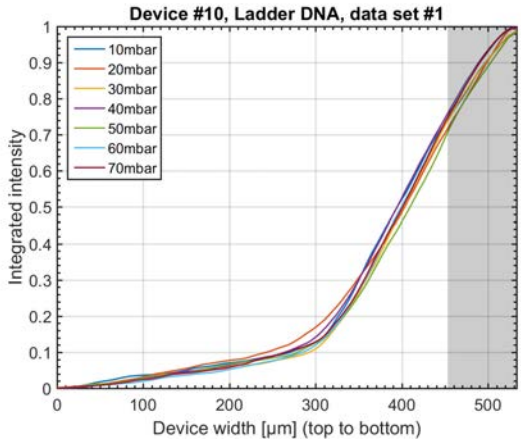

Figure 5.5: Cumulative plot for Ladder DNA in device #10, data set #1.

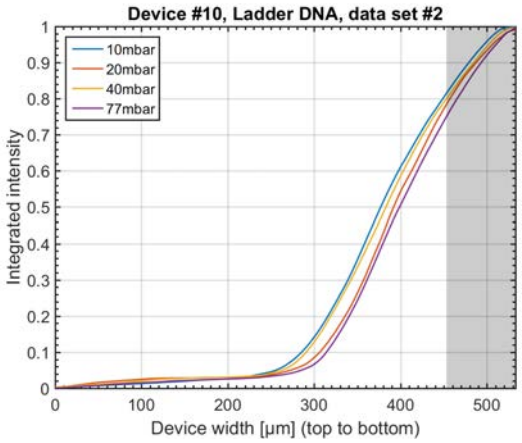

Figure 5.6: Cumulative plot for Ladder DNA in device #10, data set #2.

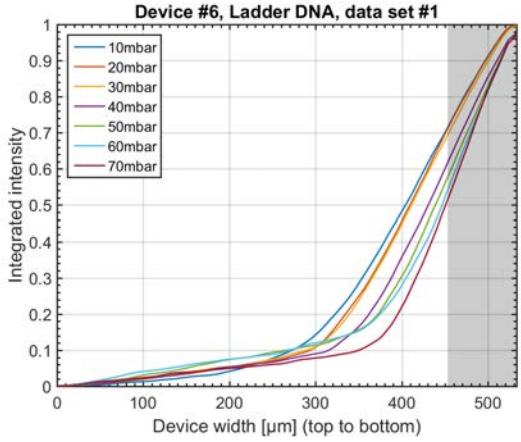

Figure 5.7: Cumulative plot for Ladder DNA in device #6, data set #1.

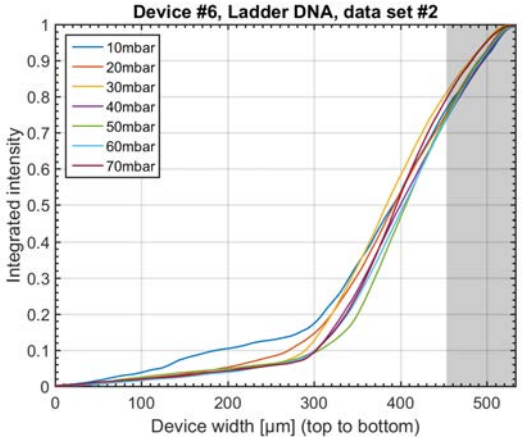

Figure 5.8: Cumulative plot for Ladder DNA in device #6, data set #2.

The separation results for Ladder DNA, as presented in Figures 5.5 - 5.8 demonstrate that Ladder DNA transits the device mainly in *zigzag* mode and does not get displaced in both devices. Though, considerable broadening occurs.

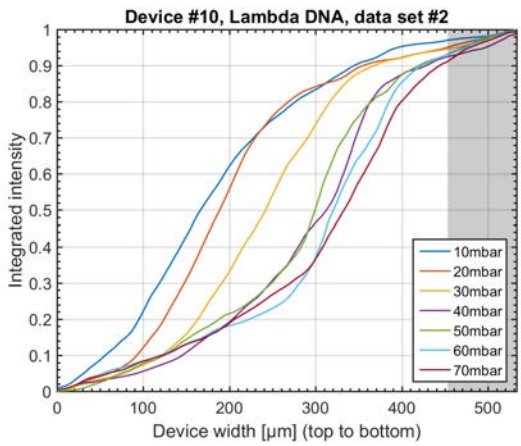

Figure 5.9: Cumulative plot for Lambda DNA in device #10, data set #1.

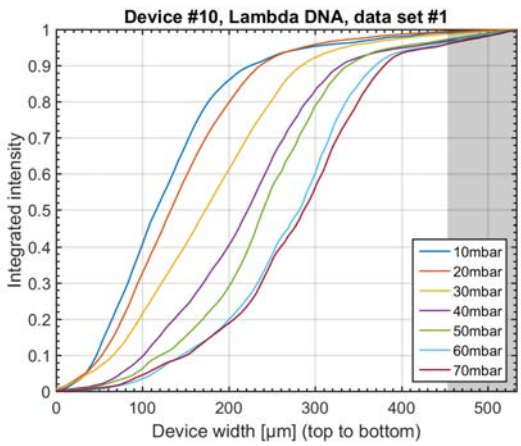

Figure 5.10: Cumulative plot for Lambda DNA in device #10, data set #2.

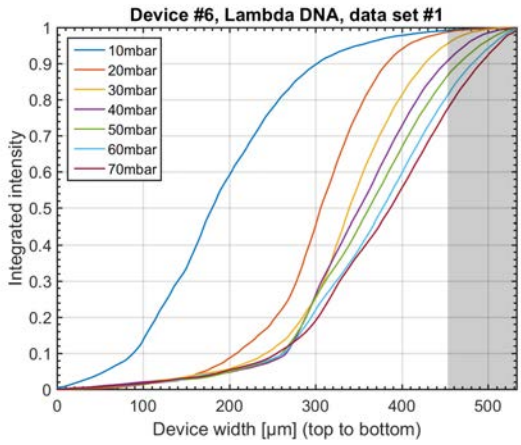

Figure 5.11: Cumulative plot for Lambda DNA in device #6, data set #1.

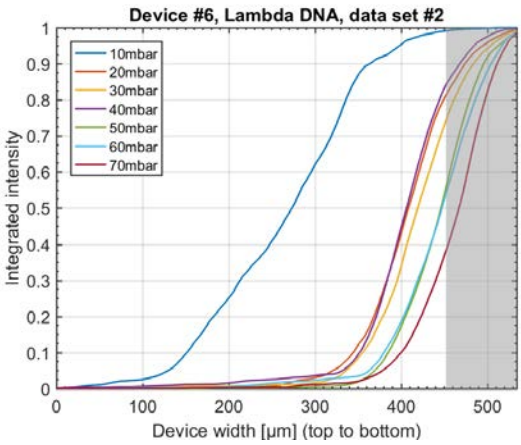

Figure 5.12: Cumulative plot for Lambda DNA in device #6, data set #2.

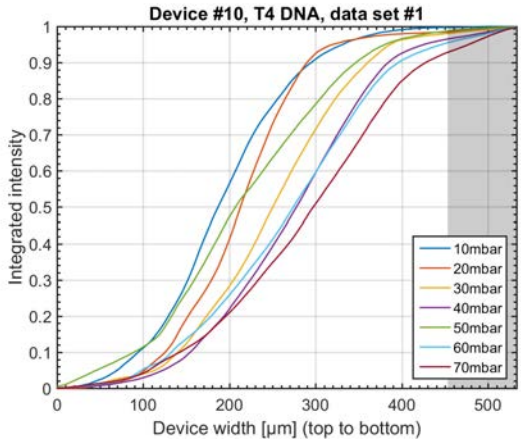

Figure 5.13: Cumulative plot for T4 DNA in device #10, data set #1.

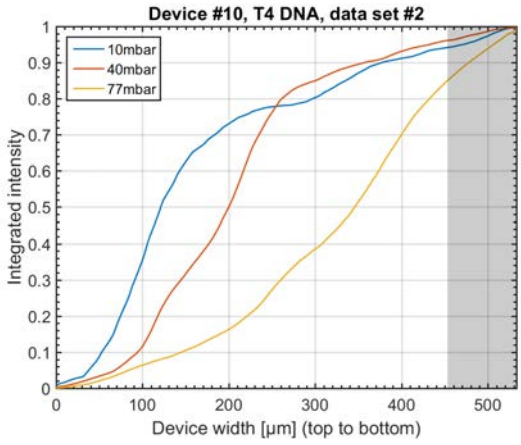

Figure 5.14: Cumulative plot for T4 DNA in device #10, data set #2.

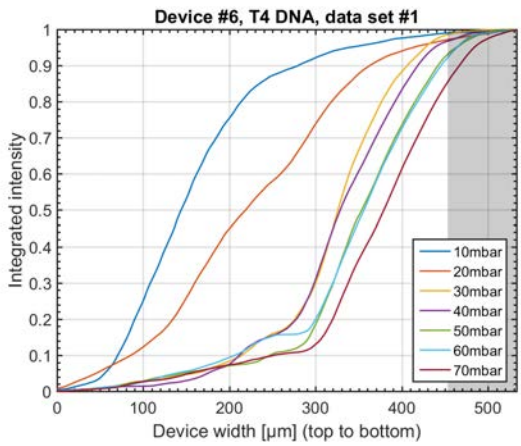

Figure 5.15: Cumulative plot for T4 DNA in device #6, data set #1.

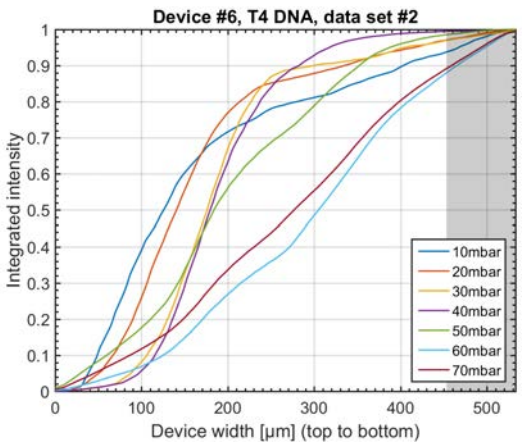

Figure 5.16: Cumulative plot for T4 DNA in device #6, data set #2.

The separation results for Lambda DNA as displayed in Figures 5.9 - 5.12 demonstrate clearly that Lambda DNA shows displacement, in both tested devices. The same holds for T4 DNA for which the results are shown in Figures 5.13 - 5.16. Notably, the results of both, Lambda and T4 DNA, show an explicit pressure dependence namely that increased pressure, *i.e.* increased velocity leads to decreased displacement.

Similar to Ladder DNA, the sample stream of Lambda and T4 DNA also undergoes a broadening while passing through the device.

5.2.2 Length dependent results

In order to directly compare the behavior and deduce how well DNA of different lengths can be separated, their cumulative functions for the same device and pressure are plotted into one graph. Those graphs are shown in Figures 5.17 - 5.22 for which only data sets #1 were considered. In the plots the positions of the device outlets are marked by dashed lines.

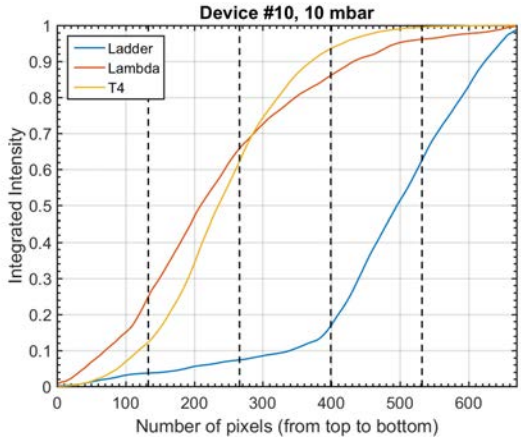

Figure 5.17: Cumulative plot showing all DNA types in device #10 at 10 mbar pressure.

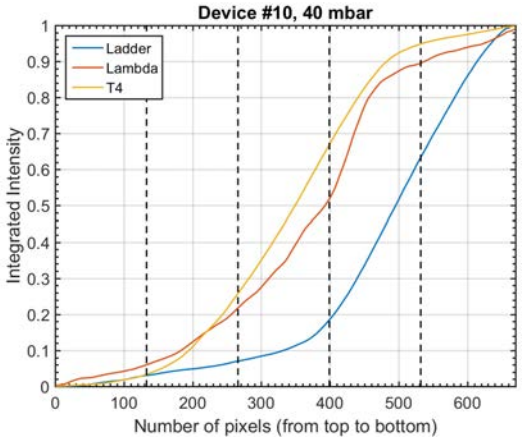

Figure 5.18: Cumulative plot showing all DNA types in device #10 at 40 mbar pressure.

The length dependent plots shown in Figures 5.17 - 5.22 prove that both tested devices are in principle capable of separating short DNA molecules such as Ladder DNA from longer DNA molecules such as Lambda and T4 DNA. The best separation is achieved at 10 mbar applied pressure.

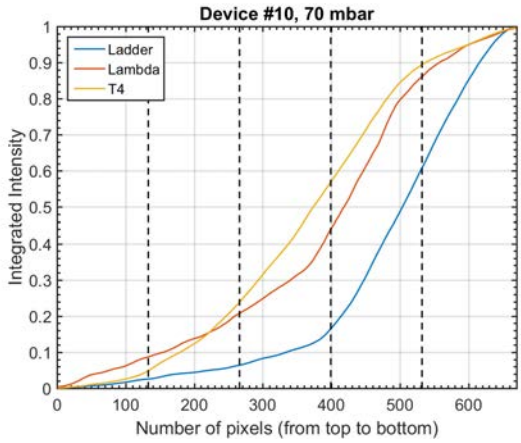

Figure 5.19: Cumulative plot showing all DNA types in device #10 at 70 mbar pressure.

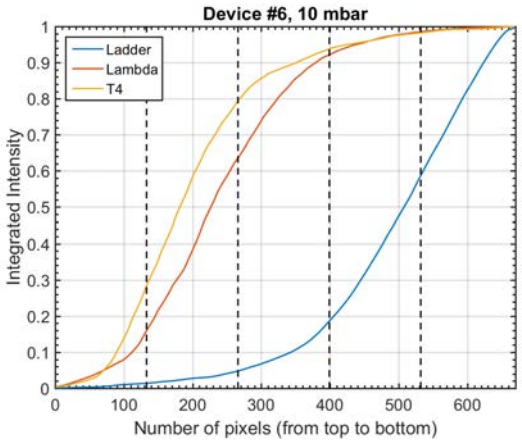

Figure 5.20: Cumulative plot showing all DNA types in device #6 at 10 mbar pressure.

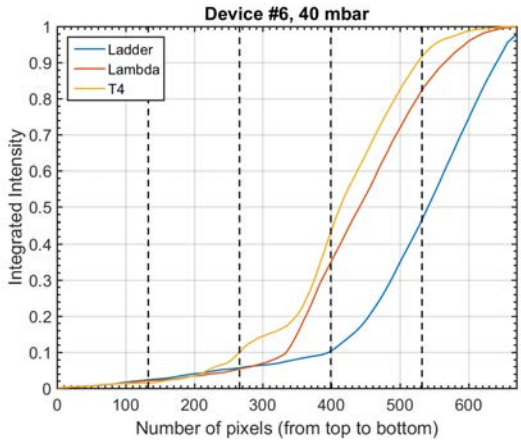

Figure 5.21: Cumulative plot all DNA types in device #6 at 40 mbar pressure.

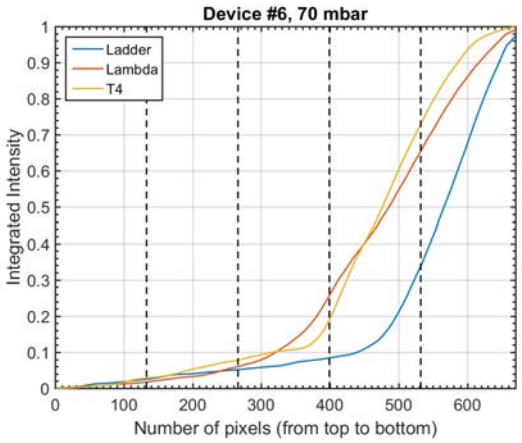

Figure 5.22: Cumulative plot showing all DNA types in device #6 at 70 mbar pressure.

5.3 Nanochannel results

The objective of the nanochannel experiments was to determine the length distribution of the Lambda and T4 DNA samples which were used in the DNA separation experiments to be able to correctly interpret the separation results. For both, Lambda and T4 DNA, about 100 movies with 100 frames each, similar to Figure 3.8 (*right*), were recorded. The MATLAB program MeltingCBAnalysis, which was developed by Tobias Ambjörnsson's group at Lund University was used for image analysis. It detects the single DNA molecules and measures their lengths. Due to time and computational limitations the length was determined by thresholding which yields only a rough estimate but is sufficient to determine if the actual length distribution agrees with the nominal length of the DNA sample.

The lengths of roughly 600 molecules were determined for both samples and the resulting length distributions for Lambda and T4 DNA are plotted in Figures 5.23 and 5.24 respectively. Consulting Equation 2.4 and assuming an effective width $w_{\text{eff}} = 5$ nm, one can find that the nominal lengths of 48.5 kbp and 165.6 kbp correspond to 4.01 μm and 13.71 μm lengths under confinement for Lambda and T4 DNA respectively. Those expected values are indicated with orange lines in the histograms.

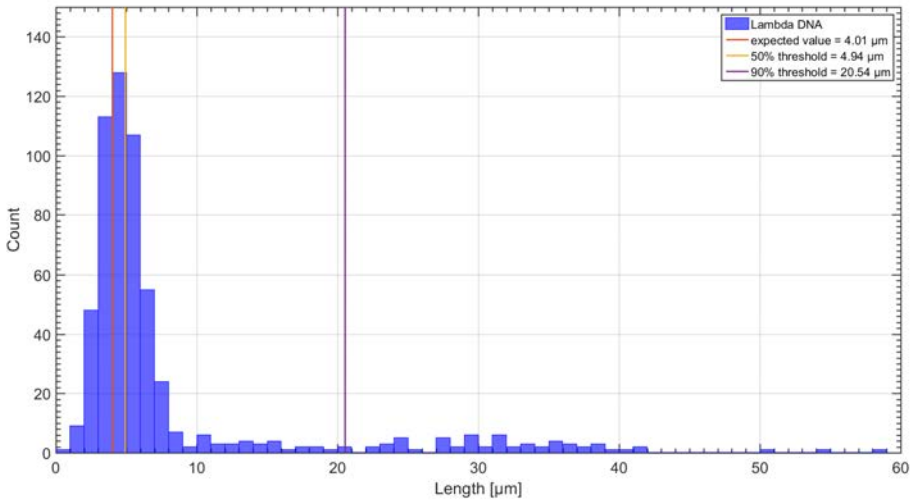

Figure 5.23: Histogram of length distribution of Lambda DNA as measured in nanochannel experiments. It shows a distinct Gaussian distribution with a median around $\simeq 5$ μm (yellow line). This is in reasonable agreement with the expected value (orange line). Though, 69% of the molecules are found to be longer than the expected length.

Looking at the length distribution of Lambda DNA as shown in Figure 5.23, one can discern a Gaussian distribution centered around $\simeq 5$ μm. It also shows a few counts for longer DNA molecules mainly around $\simeq 30$ μm but more than 90% of the measured molecules are shorter than 20.54 μm. Furthermore, the theoretically predicted value of 4.01 μm agrees reasonably well with the median of the distribution which is found to be 4.94 μm. However, 69% of the molecules are longer than the expected length. Nevertheless, the result shows, that the majority of the Lambda DNA molecules in the sample appear to be close to the nominal length of 48.5 kbp and the formation of concatemers happened only rarely.

While the length distribution of T4 DNA, as shown in Figure 5.24, also exhibits a Gaussian-shaped profile, it features a more pronounced tail with a significant number of counts up to roughly 20 μm. Still, 90% of the molecules are shorter than 23.92 μm. The median can be located at 5.98 μm which stands in disagreement to the expected value of 13.71 μm. Indeed, 78% of the molecules are found to be shorter than the expected length. This result suggests that the majority of the DNA molecules in the T4 sample have been broken up into shorter pieces. This could in principle be due to shear forces exerted on the molecules for example during pipetting or due to contamination with enzymes which break up the DNA (DNAase). Since the DNA sample has been handled with great caution in the lab, it has to be assumed that the it was already in deficient condition upon purchase.

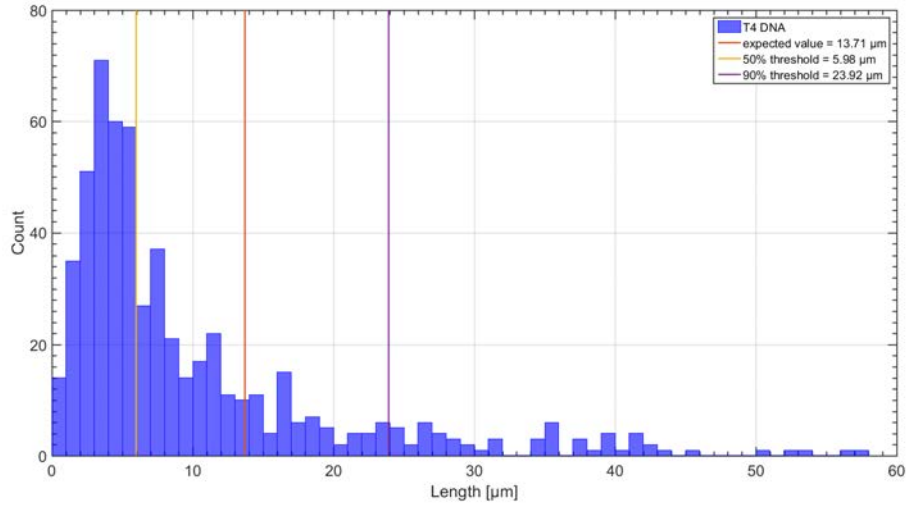

Figure 5.24: Histogram of length distribution for T4 DNA as measured in nanochannel experiments. It shows a Gaussian distribution with a pronounced tail. The median lies around $\simeq 6$ μm (yellow line) in considerable distance to the expected value (orange line). Indeed, 78% of the molecules are smaller that the expected value.

Comparing Figures 5.23 and 5.24 it can be concluded that the actual lengths of the Lambda and T4 DNA molecules are very similar. While the nominal length of T4 DNA is more than three times longer than Lambda DNA, only a length difference of approximately 20% could be observed.

5.4 Discussion

In the following section, the presented results will be analyzed and discussed. For the interpretation of the results many of the theoretically introduced concepts from Chapter 2 will become relevant.

Firstly it has to be mentioned, that the length distributions measured in the nanochannel experiments are consistent with the results from the separation experiments. The length distributions of the Lambda and T4 DNA samples were found to be quite similar which stands in agreement to the similar behavior in the separation experiments.

The effect of diffusion and structural fluctuations

As described in Section 5.2, a considerable broadening of the sample stream is observed. Since the relevant length scales of the experiments are on the μm scale, diffusion has to be considered. Table 5.1 gives the expected diffusion constants and the resulting maximum diffusion lengths for all DNA samples, calculated using Equations 2.15 and 2.16. Note, that the maximum diffusion length occurs at the lowest velocity, i.e. pressure. The calculated values show that only for the very smallest fragments of Ladder DNA diffusion might have a noticeable effect. Indeed, for Lambda and T4 DNA, the expected broadening due to diffusion is only about one post wide. However, these theoretically values are based

on the nominal molecule lengths. As the nanochannel measurements suggest, it has to be assumed that even the Lambda and T4 DNA samples contain some short DNA fragments which can cause a slight broadening.

Table 5.1: Expected diffusion constants and lengths for all DNA samples. The maximum diffusion length is given in μm and in the corresponding post width. Note that the maximum diffusion length occurs at the lowest applied pressure and the transition time through the device was assumed to be seven minutes.

	Ladder	Lambda	T4
D [m^2/s]	$3.5 \cdot 10^{-12}$ - $4.2 \cdot 10^{-13}$	$1.6 \cdot 10^{-13}$	$7.9 \cdot 10^{-14}$
r_{max} [μm]	54.2 - 18.8	11.6	8.1
r_{max} [posts]	3.0 - 1.0	0.6	0.5

Those theoretical expectations can be supported analyzing the results shown in Figures 5.5 - 5.8. Ladder DNA shows almost constant results over the probed pressure range, *i.e.* exhibits a velocity independent behavior. This proves that diffusion cannot have a large effect for Ladder DNA in the probed pressure range. As diffusion is inversely proportional to the particle size and Ladder DNA contains the shortest, *i.e.* smallest investigated DNA molecules, this holds true for the other DNA samples as well. It can be concluded that diffusion is at the most responsible for a slight broadening of the sample stream and cannot be solely responsible for it.

To further examine the reason for the observed broadening, one should have a closer look at the statistical nature of a DNA molecule's conformation. As described in Section 2.1, DNA in solution adopts the shape of a random coil. This is however only an expression for the time and ensemble average. The actual conformation of a DNA molecule at any given point in time might be very different from the random coil, since every component in the polymer chain undergoes thermal fluctuations causing structural fluctuations in the whole DNA molecule.
The sorting mechanism of a DLD device is based on a particle's size. This is straightforward for spherical particles since their size is independent of their orientation. However, when dealing with a non-spherical particle, the particle's dimension perpendicular to the flow is the one relevant for sorting. Therefore, it is also referred to as the effective size.

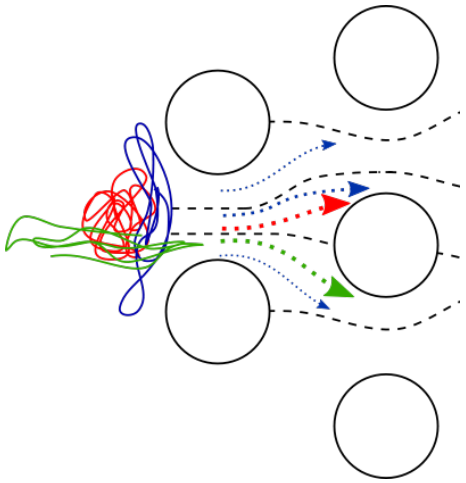

Figure 5.25: Illustration of different possible DNA conformations at encounter with posts in DLD indicating the resulting trajectories in the device. The random coil conformation is depicted in red. Other shapes which might occur due to fluctuations are depicted in green and blue. The flow is going from left to right.

As thermal fluctuations alter the random coil shape of a DNA molecule, its effective size for sorting can decrease as well as increase. Figure 5.25 shows three different possible conformations of the same DNA molecule: an ideal random coil conformation which is depicted in red and two heavily altered conformations, depicted in green and blue.

Now, it shall be considered how DNA molecules of the same length but different conformation behave when passing through a DLD device. An ideally coiled molecule behaves like a spherical particle and if its diameter is larger than the critical diameter of the device D_c (as red in Figure 5.25), it will be displaced. A molecule whose dimension parallel to the direction of flow is larger than perpendicular to it shows a diminished effective size and might in extreme cases (as green in 5.25) not be displaced even though its diameter is larger than D_c. The other way round, if the dimension of a molecule perpendicular to the direction of flow is much larger than parallel to it, the molecule is stretched over two or more streamlines and the center of mass decides which streamline the molecule will follow. The blue molecule in Figure 5.25 will most likely follow the central streamline and be displaced even though there are slim chances for no or enhanced displacement. The described trajectories of the DNA molecules are also indicated with arrows in Figure 5.25.

Note however, that the change in conformation due to thermal fluctuations is a highly dynamic process. This means that by the time the DNA molecules in Figure 5.25 have passed the next post, they could already have adopted quite different shapes. It is also important to mention, that this discussion (as well as Figure 5.25) only considered the problem as two-dimensional, whereas it is three-dimensional in reality which makes it even more complex.

In conclusion, the thermal fluctuations in the shape of a DNA molecule add a stochastic component to the experiment. This means that, when handling soft polymers, the displacement does not occur on an entirely deterministic basis as intended by the DLD theory. The superposition of deterministic and stochastic behavior also provides a reasonable explanation for the observed broadening.

The effect of shear stress and the relevance of relaxation time

As mentioned previously, the results of the DNA separation experiments suggest that the displacement of long DNA molecules decreases as the applied pressure increases. This can for example very nicely be discerned from Figure 5.9. The observed pressure dependency is surprising at first glance since the DLD mechanism itself is independent of the flow velocity. Although, one has to bear in mind that the theory behind DLD assumes rigid spheres and even though a DNA molecule in solution can in first approximation be considered spherical, the deformability of a DNA molecules is where the discussion on the pressure dependency has to start.

Obviously, there is at least one additional effect coming increasingly into play at higher flow velocities which prevents separation. As described in Section 2.1, shear forces induced by fluid flow can cause DNA molecules to extend in the direction of flow and the elongation scales with the applied force. Consequently, an increase in flow velocity results in a higher shear force and thus enhanced elongation. Again, elongation results in the decrease of the effective size of the DNA molecule. Thus, there is a critical shear force S_c above which not displacement will occur since the effective size of the DNA is smaller than the critical diameter D_c of the DLD device. However, it is important to realize that a constant shear stress as supplied by the fluid flow does not result in a complete expansion of the DNA molecule but rather causes the time averaged conformation of the DNA molecule to be an ellipsoid with the major axis along the direction of flow.

Nevertheless, the constant shear stress due to the fluid flow is not the only effect which has to be considered. Interactions between the DNA molecules and the posts or device walls happen frequently. Those interactions are typically induced by a collision of a DNA molecule with a post or device wall. DNA-device interaction which have been observed during the experiments are **(a)** the crashing of the DNA molecule into the post, **(b)** the entanglement of the DNA molecule around a post, forming a U-shape (also described by [31]), and **(c)** the sticking or partial sticking of the DNA molecule to the posts or the device walls.

All three mentioned interactions result in either partial or complete extension of the DNA molecule. In the case of **(a)** this is due to the non-uniform velocity profile around a post which means that deformed DNA molecule after colliding with a post experiences a strong velocity gradient which results in the expansion of the molecule. For **(b)** and **(c)**, parts of the molecule are constrained which likewise results in the expansion of the molecule.

However, as mentioned in Section 2.1, a stretched out DNA molecule tends to coil back into its random coil conformation. If this recoiling happens before the DNA molecule encounters the next post, the effective size of the DNA as well as the displacement behavior would be unaffected. Whereas, if the DNA molecule is still considerably stretched at the encounter with the next post is has a largely diminished effective size most likely no displacement will occur.

Thus, two time regimes are defined. Firstly, the relaxation time of the DNA coil, τ_{DNA} as defined in Equation 2.5, and secondly the transition time between two posts τ_{trans}, which is defined as

$$\tau_{\mathrm{trans}} = \frac{\lambda}{v}, \tag{5.1}$$

where λ is the distance between the posts and v is the flow velocity. The case $\tau_{\mathrm{DNA}} \ll \tau_{\mathrm{trans}}$ is termed *markovian* as the molecule is 'memoryless' and had sufficient time such that its future is independent of previous processes. On the other hand, for $\tau_{\mathrm{DNA}} \gg \tau_{\mathrm{trans}}$, the *non-markovian* case, the DNA molecule is still stretched out from the previous interaction and this will influence the next displacement process.

Table 5.2: Estimates for the relevant time scales for Lambda DNA.

$\tau_{\mathrm{DNA,\ Lambda}}$	0.11 s
$\tau_{\mathrm{trans,\ 10mbar}}$	$\simeq$ 0.25 s
$\tau_{\mathrm{trans,\ 70mbar}}$	$\simeq$ 0.036 s

Table 5.2 contains estimates for the relevant time scales where the values for τ_{trans} are rough approximations. The numbers show that for Lambda DNA at 10 mbar $\tau_{\mathrm{DNA}} \ll \tau_{\mathrm{trans}}$ whereas at 70 mbar $\tau_{\mathrm{DNA}} \gg \tau_{\mathrm{trans}}$. This means that due to the markovian behavior, the displacement at 10 mbar is unaffected by the DNA-post interactions. In contrast, at 77 mbar the behavior is non-markovian and the DNA molecule travels about three posts before is recoils assuming that no new interactions occur meanwhile. While passing those post the DNA molecule will be extended and have a smaller effective size and displacement is prohibited.

Concluding, the decreased displacement at higher pressure can be accounted for by the decrease in the DNA's effective size resulting in prevented displacement. The decrease in effective size may be caused by increased shear forces at higher velocities and the subsequent elongation and by the decrease of τ_{trans} which causes the relaxation behavior after DNA-post interactions to shift into a non-markovian regime.

Different critical sizes D_c

It is also interesting to analyze whether the critical diameter of the DLD device has an influence on the sorting. For this, the performance in the two tested devices can be compared, recalling that the critical diameters of devices #6 and #10 are 0.75 μm and 0.64 μm respectively. In Figures 5.26 and 5.27, the position of the median (circles) is plotted against the applied pressure for all three DNA samples. The bars indicate the 20% spread from the median to each side thereby cover the range at which the central 40% of the sample exits the device.

The plots show nicely that the position of the median converges for the three DNA types at higher pressure, indicating decreasing displacement of Lambda and T4 DNA. Furthermore, it is clear that this convergence occurs is faster and at lower pressures for device #6, *i.e.* at a larger critical diameter. This result agrees with the previous discussion on shear stress and diminished effective size since for a device with smaller critical radius, a higher level of elongation has to be reached to prevent the molecules from displacing.

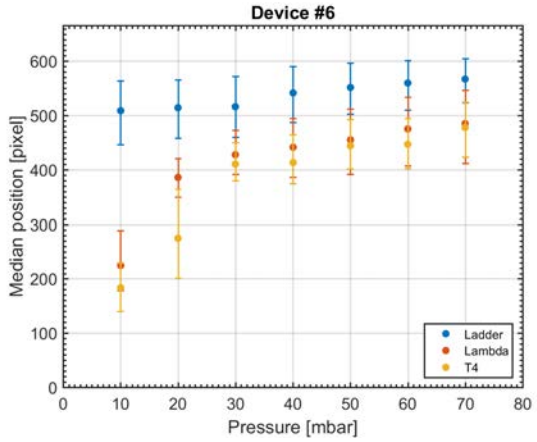

Figure 5.26: Plot of the median position of the DNA at outlet plotted against the pressure for device #6. The bars cover the 20% spread from the median to each side.

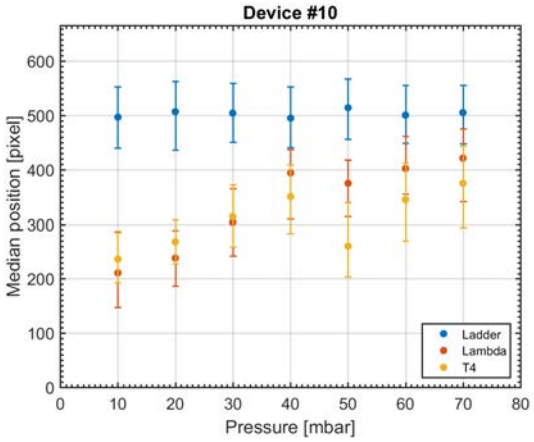

Figure 5.27: Plot of the median position of the DNA at outlet plotted against the pressure for device #10. The bars cover the 20% spread from the median to each side.

It is also interesting to mention that a device with critical diameter $D_c = 1.00$ μm has briefly been tested and no displacement could be observed for Lambda or T4 DNA in the tested pressure range.

Quality of separation

Finally, the achieved quality of separation shall be analyzed. In separation experiments in general, the quality of separation is typically measured by purity which was achieved.

The purity is an expression for the relative amount or concentration of the desired particle or molecule after the separation.

Figures 5.28 and 5.29 show the calculated purities for Lambda DNA relative to Ladder DNA at the different outlets of device #6 and #10 respectively. For the calculation of the cumulative data from Figures 5.20 - 5.19 was used and it was assumed that the detected intensity corresponds directly to the amount of DNA sample.

The tested devices have five outlets which are distributed evenly over the width of the device. Their boundaries are marked with dashed lines in Figures 5.28 and 5.29. All fluid and sample leaving the device through the same outlet is also collected in the same reservoir. Therefore, the purity can only be considered over the whole width of one outlet.

Figures 5.28 and 5.29 show that for both devices, Lambda DNA can be separated from Ladder DNA with a purity $> 93\%$. The best separation quality is achieved in the second upper most outlet at 10 mbar. However, which of the outlets is best depends on the applied pressure. The plots also demonstrate that device #10 is generally better suited for separation since it yields better purity at a wider range of parameters.

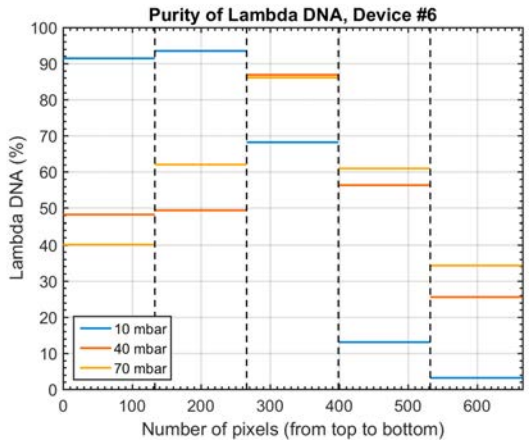

Figure 5.28: Plot of the separation purity of Lambda DNA over the five outlets of device #6. The values correspond to the relative amount of Lambda DNA compared to Ladder DNA.

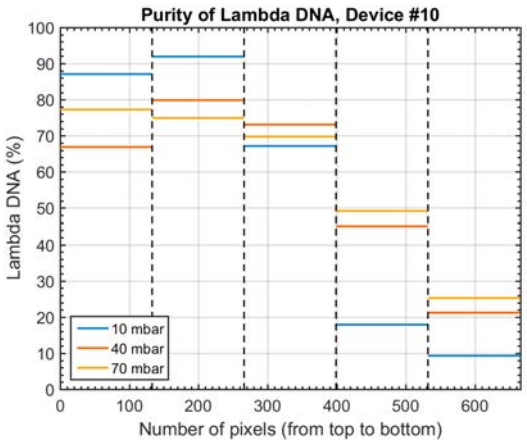

Figure 5.29: Plot of the separation purity of Lambda DNA over the five outlets of device #10. The values correspond to the relative amount of Lambda DNA compared to Ladder DNA.

Chapter 6

Conclusions and Outlook

This thesis investigated whether the method of DLD can be used to separate DNA molecules by length. For this, microfluidic DLD devices with critical diameters D_c 0.64 μm and 0.75 μm respectively were fabricated in PDMS using soft lithography methods. Three different DNA samples of the nominal lengths <10 kbp (Ladder), 48.5 kbp (Lambda) and 165.6 kbp (T4) were fluorescently labeled with the dye YOYO®-1. Experiments for every device and sample combination were carried out using pressure driven flow to transport the sample through the device. The final position of the sample at the device outlet was observed using epi-fluorescence microscopy. The recorded movies were subsequently evaluated by carefully devised image analysis.

It was found, that the two probed DLD devices can indeed be used to separate <10 kbp from 48.5 kbp DNA molecules. This confirms the findings of Huang *et al.*, [6], and shows additionally that pressure driven flow can be used as transport mechanism. Furthermore, it proves that the separation range can be modified such that very small particles (sub-μm) or DNA fragments can be separated from long DNA molecules. In order to achieve high separation purity, the pressure range, *i.e.* flow velocity has to be tuned carefully and the critical diameter of the DLD device has to be adjusted to the desired separation range. At low applied pressure a sample purity of $\simeq 94\%$ was achieved.

It was furthermore discussed how diffusion, thermal fluctuations, shear stress and relaxation time influence the displacement process. At low pressure, diffusion can have a large effect and might ruin the separation. On the other hand, at high pressure shear stress and a smaller transition time, *i.e.* a smaller relative relaxation time can decrease the effective size of the DNA and prevent displacement. Moreover, thermal fluctuations constantly change the shape of the DNA molecule and introduce therefore a stochastic component to the DLD mechanism.

As explained, different effects are of varying importance in different regimes. However, one has to keep in mind that all the described effects are present at all times and their superposition determines the actual dynamics of a DNA molecule its resulting behavior in a DLD device. The provided discussion tried convey which effects are dominating in certain regimes and attempted to explain which concrete consequences this had in the conducted experiments. However, from the perspective of DNA polymer physics, the problem of DNA in a DLD deice is immensely complex. The here presented experiments do allow to catch a glimpse at the qualitative nature of the problem but do not suffice for a thorough and quantitative analysis of the problem.

Now, two concrete follow-up experiments shall be proposed and the future directions and prospects shall be illustrated.

Firstly, it has been shown that the DNA persistence length and thus also the radius and the deformability of the DNA coil is dependent on the salt concentration of the solvent [56]. It has also recently been demonstrated that by changing the salt concentration in a DLD device the critical diameter D_c can be modulated [57]. Literature suggests that an increased salt concentration results in a smaller and more rigid DNA coil. It would therefore be interesting to run experiments in the same device, at the same pressure and with the same DNA sample but at varying salt concentrations to determine whether this can indeed change the displacement behavior. The idea could then be even taken one step further and a DLD device with several extra inlets across the length of the array could be fabricated. By inserting solvents of different salt concentrations at several stages one device could be used for sorting of multiple DNA molecules with a dynamical separation range.

Secondly, to further investigate the dynamics of the DNA molecules in the DLD device one could repeat the conducted experiments using high resolution microscopy. Better resolution would allow to directly observe single DNA molcules and their DNA-post interactions. It would also be possible to correlate which the different kinds of DNA-post interactions with the resulting trajectories. This would generate a more direct cause-action scheme and allow a deeper insight into the relevant polymer physics of DNA. It would furthermore be interesting to investigate a larger pressure range in order to better define the diffusion- and shear stress dominated regimes in which no separation can be achieved.

Certainly, there are also problems with the presented approach which have to be resolved to make it convenient and easier to use. The most important problem is the sample extraction after the separation process. Currently it is not possible to extract the collected DNA molecules from the outlets for imaging or further experiments. This is mainly due to technical difficulties with pipetting and the small handled sample volumes. However, this problem could be overcome by implementing an integrated DLD and nanofluidic device in which each displaced DNA molecule is directly pulled into a nanochannel. This is one of the upcoming research projects in Jonas Tegenfeldt's group.

An integrated DLD-nanofluidic device would permit to directly measure the length of a captured DNA molecule. It would also allow the integration with optical mapping which is a simple technique for the determination of the so called barcode of a DNA molecule. The DNA barcode is unique to the DNA molecules sequence which makes sequence identification possible. This could ultimately allow the fabrication of an integrated system, where a cell is first lysed, then flushed into a DLD device which displaces the DNA (and only the DNA) into a nanochannel array where the DNA sequence can be identified via optical mapping. Ready availability of such a system would be a milestone for molecular biology and medicine.

The proof-of-principle for DNA separation in DLD using pressure-driven flow as demonstrated in this thesis will together with applications for sample purification most likely lead to a publication.

Appendix A

Protocols

A.1 Soft lithography protocol

The following protocol describes all necessary processing steps to fabricate a microfluidic device in PDMS from a patterned silicon wafer.

1. Mixing of PDMS and curing agent in 10:1 ratio. To cover a 3" silicon wafer 5g of PDMS are sufficient. The two PDMS components need to be mixed for several minutes until they become a homogeneous mixture. The mixture is then desiccated for at least 20 minutes to make air bubbles which arose during mixing disappear. If the PDMS is free of air bubbles it is carefully poured onto the silicon wafer. Subsequently, it is baked in an oven at 80 °C for at least one hour.
2. During baking the formerly thick fluid solidifies and can be pulled off the wafer afterwards. Since the PDMS is now an imprint of the microstructures from the wafer, this should be done very cautiously to avoid ripping out tiny pieces from the PDMS which then stay on the wafer and make the PDMS mold unusable.
3. The PDMS mold is then placed on a glass slide. Typically, one silicon wafer contains the imprint of several devices, such that the desired device has to be cut out first. Then, holes are punched into the PDMS at the inlets and outlets.
4. Afterwards, the PDMS device is flipped upside down and inserted into the plasma oven, together with a glass slide. The details of the plasma treatment protocol are described in the appendix.
5. Afterwards, the PDMS device and the glass slide are taken out from the plasma oven and put on top of each other such that the two to the plasma exposed surfaces can bond. It is important to fill the device with water directly after the boding since the microfluidic channel is only hydrophilic for a short time after the plasma treatment. The channel should be filled from only one side to avoid air getting trapped in the middle.
6. Subsequently, short plastic tubes which serve as inlet and outlet reservoirs are glued on top of the holes which have been punched prior to plasma treatment. This is done using ELASTOSIL® A07 by Wacker, a solvent-based silicon dispersion which cures at room temperature [58].

A.2 Staining protocol

The smallest possible volume to pipette is 1μl, which is therefore base unit in the following protocols. Note, that when pipetting solutions containing DNA, pipettes with a wider or cut-off tip have to be used to minimize the shear forces acting on the DNA molecules. The stock concentrations of the concerned ingredients were:

- YOYO®-1 : $c_{0,\mathrm{YOYO}} = 1$ mM,
- Ladder DNA: $c_{0,\mathrm{Ladder}} = 0.5$ μg/μl,
- Lambda DNA: $c_{0,\mathrm{Lambda}} = 0.5$ μg/μl,
- T4 DNA: $c_{0,\mathrm{T4}} = 0.32$ μg/μl.

Ladder and Lambda

1. The stock concentrations of Ladder and Lambda are $c_{0,\mathrm{Ladder}} = c_{0,\mathrm{Lambda}} = 0.5$ μg/μl, which corresponds to a molar concentration of 0.76 mM.
2. To obtain a volume ratio of 1:1 and a molar ratio of 10:1, the concentration of YOYO®-1 has to be $c_{1,\mathrm{YOYO}} \stackrel{!}{=} 0.076$ mM.
3. Thus, a YOYO®-1 dilution containing 12.15 μl DI water and 1 μl YOYO®-1 ($c_{0,\mathrm{YOYO}}$) is prepared.
4. Finally, 1 μl of Ladder or Lambda ($c_{0,\mathrm{Ladder}}/c_{0,\mathrm{Lambda}}$) and 1 μl of YOYO®-1 ($c_{1,\mathrm{YOYO}}$) are mixed.

T4

1. The stock concentrations of T4 is $c_{0,\mathrm{T4}} = 0.32$ μg/μl, which corresponds to a molar concentration of 0.48 mM.
2. Accordingly, the concentration of YOYO®-1 has to be $c_{2,\mathrm{YOYO}} \stackrel{!}{=} 0.048$ mM.
3. Thus, a YOYO®-1 dilution containing 19.83 μl DI water and 1 μl YOYO®-1 ($c_{0,\mathrm{YOYO}}$) is prepared.
4. Finally, 1 μl of T4 ($c_{0,\mathrm{T4}}$) and 1 μl of YOYO®-1 ($c_{2,\mathrm{YOYO}}$) are mixed.

A.3 Protocol for conducting a DNA separation experiment

The following protocol gives a thorough description of all steps which are necessary to conduct a DNA separation experiment.

1. The microfluidic device is mounted on the microscope stage and the white lamp is used to adjust the focus.

2. DI water in the inlet and outlet reservoirs is replaced by buffer solution (0.5x TAE, 1% BME). The Fluigent is connected to the inlets to flush the device with buffer solution to ensure homogeneous conditions within.

3. During the flushing process, the device is checked for air bubbles since any air contained in the device will disturb or hinder the fluid flow.

4. If the device is completely filled with buffer, the DNA sample is loaded into the correct inlet tube. A moderate pressure is applied to inject the sample into the device.

5. The white lamp is switched off to be able to observe the fluorescent light emitted by the sample. To improve the image quality, stray light coming from other light sources should be eliminated.

6. The pressures applied to the sample and buffer inlet are balanced such that the streams flow in parallel when entering the device as shown in Figure 3.6.

7. To record the separation result, movies with 800 frames are taken at the outlet of the device. Note, that after adjusting the pressure at the inlet it is crucial to wait for at least one translation period before recording the result at the outlet. A typical image at the outlet is shown in Figure 3.6.

When changing the applied pressure, steps 6 and 7 of the protocol have to be repeated.

A.4 Protocol for conducting a nanochannel experiment

The following protocol gives a thorough description of all steps which are necessary to conduct nanochannel experiment.

1. The plastic cover of the nanofluidic device is carefully unscrewed and the four reservoirs belonging to one device are filled with fresh buffer solution (0.5x TAE, 1% BME). For the pipetting a metal syringe tip is used instead of the usual plastic tips.

2. The device is mounted on the microscope stage. The four pressure tubes from the pressure control system are connected to the reservoirs. This is usually done such that the pressure channels numbered as 1 & 2 and 3 & 4 each are connected to the same microchannel. The numbering is consistent with the number shown on the reservoirs in Figure 3.4.

3. The pressure on channels 1 and 3 is switch on to flush the microchannels with buffer. Then, channel 3 is switched off and channel 2 is switched on to flush the nanochannels with buffer.

4. After the whole device has been flushed with buffer it is disconnected from the pressure tubes, unmounted and the cover is unscrewed. The buffer solution in reservoir 1 is replaced with the DNA sample.

5. The nanofluidic device is again correctly mounted on the microscope stage and connected to the pressure tubes. The white lamp is used to adjust the focus. If the 60x oil immersion objective is used, make sure there is an oil film between the objective and the bottom of the device.

6. Then, the pressure on channels 1 and 3 is switched on and the DNA is transported through one of the microchannels. To image the DNA, the white lamp is switched off and the power of the lamp is reduced to 1% power to minimize the photodamage.

7. To ensure a sufficiently high concentration of DNA molecules upon entry into the nanochannels, the molecules can be accumulated at the entry region by additionally switching on the pressure on channel 2. During this accumulation process it is advisable to keep the lamp off completely to ensure that the DNA molecules which are about to enter the nanochannels are undamaged.

8. To force the DNA molecules into the nanochannels one has to apply a pressure pulse. This can be done by manually closing a leak at the pressure control board. Then, the pressure is turned off completely and the DNA molecules remain at their current position within the nanochannels and can be imaged.

9. To image the molecules the lamp is switched on to 100% power and movies with 100 frames are taken.

To obtain good statistics many molecules have to be measured. For this, steps 6 - 9 of the protocol have to be repeated.

Appendix B

Matlab Code

B.1 CalculatingQuantileFunc

```
1  function [] = CalculatingQuantileFunc( FolderName, Quantile,
       SampleNum )
2
3  FullPath = [FolderName '/*.tif'];
4  FileInfoAll = dir(FullPath); % gives out a structure containing
       names and other information about all files contained in the
       given folder
5
6  for v=1:length(FileInfoAll)
7
8      FileInfoCurrent = FileInfoAll(v); % gives out a structure
           containing information about file i
9      FileNameCurrent = FileInfoCurrent.name; % gives out a string
           containg the name of file i
10     FileIn = strcat(FolderName,'/',FileNameCurrent); % generates
           the complete path of file i
11
12     InfoImage = imfinfo(FileIn);
13     mImage = InfoImage(1).Width;     % read out image width
14     nImage = InfoImage(1).Height;    % read out image height
15     NumberImages = length(InfoImage);    % read out number of
           frames in stack
16
17     FinalImage = zeros(nImage,mImage,NumberImages,'uint16');
18     for i=1:NumberImages
19         FinalImage(:,:,i) = imread(FileIn,'Index',i); % load
               stack into 3dim matrix FinalImage
20     end
21
22     randNum = round(NumberImages*SampleNum);
23     randVec = randi([20 NumberImages],randNum,1); % generate
```

```
        randNum of random numbers between 20 and NumberImages
24
25      quantMatrix = zeros(nImage,mImage,'uint16');
26      vec = zeros(randNum,1);
27      vec_sorted = zeros(randNum,1);
28
29      % The following loop goes into every pixel of the stack and
            loops
30      % through the z-direction writing all intensity values into
            vec. Those
31      % are then sorted in vec_sorted. The intensity value at the
32
33      for i=1:mImage
34          for j=1:nImage
35              for k=1:randNum
36                  vec(k,1) = FinalImage(i,j,randVec(k,1));
37                  vec_sorted = sort(vec);
38                  quant = vec_sorted(round(Quantile*randNum));
39                  quantMatrix(i,j) = quant;
40              end
41          end
42      end
43
44      FileOutAppend = strcat('_ResultQuantian.tif');
45      FileOut = strrep(FileIn,'.tif',FileOutAppend);
46
47      imwrite(quantMatrix,FileOut)
48
49      figure
50      imagesc(quantMatrix)
51      colormap(gray)
52  end
53
54  end
```

B.2 FindingPostSize

```
1  clear all
2  close all
3
4  FolderName = 'FilesLadderBaoDevice10Date20151203';
5
6  FullPath = [FolderName '/*.tif'];
7  FileInfoAll = dir(FullPath); % gives out a structure containing
       names and other information about all files contained in the
       given folder
8
9  for w=1:length(FileInfoAll)
```

```
10
11      FileInfoCurrent = FileInfoAll(w); % gives out a structure
            containing information about file i
12      FileNameCurrent = FileInfoCurrent.name; % gives out a string
            containg the name of file i
13      FileIn = strcat(FolderName,'/',FileNameCurrent); % generates
            the complete path of file i
14      checkFile = strfind(FileNameCurrent,'Subtracted_Averaged_');
15      if checkFile==1
16          if mod(w,2) == 0
17          else
18          FileIn = strcat(FolderName,'/',FileNameCurrent);
19
20          %% Reading in image file as matrix and plotting it %%
21
22          A = imread(FileIn); % reads the pixel values into a
                matrix
23          A = double(A);
24
25          A = ImageRotationFunc(A,+5); % Calls the function to
                rotate and crop the image/matrix. Second passing
                argument is the rotation angle
26
27         %% generating matrix which sets all entries left of the
               max column to zero%%
28
29          A_array = A;
30          thresh = 2/3;
31
32          for i=1:length(A)
33              for j=1:round(length(A)*thresh)
34                  A_array(i,j)=0;
35              end
36          end
37
38        %% finding width of the posts by searching for intensity
              minima and maxima within lines/columns and finding
              their distance %%
39
40          % finding maxima in the matrix %
41          A_arrayLocalMax = vision.LocalMaximaFinder; % calling
                the maximum finder function
42          A_arrayLocalMax.MaximumNumLocalMaxima = 1000; % setting
                th number of maxima to be found
43          A_arrayLocalMax.NeighborhoodSize = [1 1]; % defining the
                 neighbourhoodsize in which only one maximum can be
                found
44          A_arrayLocalMax.Threshold = 1.25*mean(mean(A)); %
```

```
            definig the threshold which a matrix entry has to
            match or exceed to be a maximum
45
46          locationMaxInt = step(A_arrayLocalMax, A_array); %
            applying the maximum finder with defines settings to
            A_array and storing the x and y values of the maxima
            in the vector location
47          locationMaxInt = double(locationMaxInt);
48
49          % calculating the separation of the found maxima %
50
51          n1 = 1;
52          sepX = zeros(1,1);
53          sepY = zeros(1,1);
54
55          for i=1:length(locationMaxInt)-1
56              for j=(i+1):length(locationMaxInt)
57                  sepX(n1,1) = abs(locationMaxInt(i,1)-
                        locationMaxInt(j,1));
58                  sepY(n1,1) = abs(locationMaxInt(i,2)-
                        locationMaxInt(j,2));
59                  n1 = n1 + 1;
60              end
61          end
62
63          hist_sepX = hist(sepX,length(A)*(1-thresh)); % histogram
                containing the distances between the intensity
            maxima in x
64
65          %% Moving average over hist_sepX
66
67          rangeMovAvg_2 = 2; %sets the range of the moving average
                along x
68
69          %MovAvgVec = smooth(hist_x,rangeMovAvg);
70
71  %% Manual code for moving average: better at edge effects than
    built-in code %%
72
73          for i=1:length(hist_sepX)
74              k = 1;
75              vecCur_MovAvg = zeros(1,1);
76              if i<=rangeMovAvg_2 % special case: left boundary
77                  for j=1:(i+rangeMovAvg_2)
78                      vecCur_MovAvg(k,1) = hist_sepX(j);
79                      k=k+1;
80                  end
81                  hist_sepX(1,i) = mean(vecCur_MovAvg);
```

```
82
83              elseif i>(length(hist_sepX)-rangeMovAvg_2) % special
                    case: right boundary
84                  for j=(i-rangeMovAvg_2):(length(hist_sepX))
85                      vecCur_MovAvg(k,1) = hist_sepX(j);
86                      k=k+1;
87                  end
88                  hist_sepX(1,i) = mean(vecCur_MovAvg);
89
90              else % normal case
91                  for j=(i-rangeMovAvg_2):(i+rangeMovAvg_2)
92                      vecCur_MovAvg(k,1) =  hist_sepX(j); %
                            elements from hist_x within the current
                            range are written to vecCur_MovAvg
93                      k = k + 1;
94                  end
95                  hist_sepX(1,i) = mean(vecCur_MovAvg); % the
                        average of vecCur_MovAvg is calculated
96              end
97          end
98
99          %hist_sepX = smooth(hist_sepX);
100         %hist_sepX = hist_sepX';
101
102         % finding the maxima of the separation histogram
103
104         sepXLocalMax = vision.LocalMaximaFinder; % calling the
                maximum finder function
105         sepXLocalMax.MaximumNumLocalMaxima = 6; % setting th
                number of maxima to be found
106         sepXLocalMax.NeighborhoodSize = [1 15]; % defining the
                neighbourhoodsize in which only one maximum can be
                found
107         sepXLocalMax.Threshold = max(hist_sepX)/10; % definig
                the threshold which a matrix entry has to match or
                exceed to be a maximum
108
109         location_sepX = step(sepXLocalMax, hist_sepX); %
                applying the maximum finder with defines settings to
                the xhistogram and storing the x and y values of the
                maxima in the vector location
110         location_sepX = double(location_sepX);
111
112         % calculating the distance between the peaks in the
                histogram, i.e. the
113         % width of one repeating unit in the array, or how far
                wo post centers are
114         % apart
```

```
115
116         n2 = 1;
117         for i=1:length(location_sepX)-1
118             for j=(i+1):length(location_sepX)
119                 postDist_vec(n2,1) = abs(location_sepX(i,1)-
                        location_sepX(j,1))/abs(i-j);
120                 n2 = n2 + 1;
121             end
122         end
123
124         postDist(w) = sum(postDist_vec)/length(postDist_vec); %
            distance between the center of posts is the average
            distace between the peaks
125
126         %% Plots %%
127
128         FileNameCurrent = strrep(FileNameCurrent,'_','');
129
130         figure
131         imagesc(A)
132         colormap(gray)
133         hold on
134         scatter(locationMaxInt(:,1),locationMaxInt(:,2),'xr') %
            plot the found maxima as scatter plot
135         title('Found intensity maxima on right side of boundPos'
            )
136
137         figure
138         plot(hist_sepX)
139         hold on
140         scatter(location_sepX(:,1),location_sepX(:,2),'xr')
141         grid on
142         legend('Histogram plot', 'Peak locations', 'Location', '
            NorthEast');
143         xlabel('Distance [pixels]')
144         ylabel('Count')
145         xlim([0 round(length(A)*(1-thresh))])
146         title('Histogram plot of maximum intensity separation in
            x')
147
148         end
149     end
150
151 end
152
153 for i=1:length(postDist)/2+1
154     if postDist(i) == 0
155         postDist(i) = [];
```

```
156     end
157 end
158
159 postDistAvg = mean(postDist);
```

B.3 ImageRotationFunc

```
 1 function [ A_rot ] = ImageRotationFunc( A, rotAngle )
 2
 3 %% Reading in image file as matrix and plotting it %%
 4
 5 %         figure
 6 %         imagesc(A)
 7 %         colormap(gray)
 8
 9         A_rot = imrotate(A,rotAngle,'bilinear','crop');
10         A_rot = double(A_rot);
11
12         for i=1:length(A_rot)
13             for j=1:length(A_rot)
14                 A_rot(i,j)=round(A_rot(i,j));
15             end
16         end
17
18
19         %% find cutting threshold
20
21         cut1 = 0;
22         cut2 = 0;
23
24         %for positive rotation angle: cutting matrix to new dim
25
26         if rotAngle > 0
27             for i=1:length(A_rot)-1
28                 if A_rot(i,1)==0 && A_rot(i+1,1)~=0
29                     cut1 = i+1;
30                 end
31             end
32
33             A_rot(1:cut1,:) = [];
34
35             for i=1:length(A_rot)-1
36                 if A_rot(1,i)~=0 && A_rot(1,i+1)==0
37                     cut2 = i;
38                 end
39             end
40
41             A_rot(:,cut2:length(A_rot)) =[];
```

```
42              A_rot(:,1:cut1) = [];
43              A_rot((cut2-cut1):length(A_rot),:) =[];
44          end
45
46          if rotAngle < 0
47              for i=1:length(A_rot)-1
48                  if A_rot(1,i)==0 && A_rot(1,i+1)~=0
49                      cut1 = i+1;
50                  end
51              end
52
53              A_rot(:,1:cut1) = [];
54
55              for i=1:length(A_rot)-1
56                  if A_rot(i,1)~=0 && A_rot(i+1,1)==0
57                      cut2 = i;
58                  end
59              end
60
61              A_rot(1:cut1,:) =[];
62              A_rot(:,cut2-cut1:length(A_rot)) = [];
63              A_rot((cut2-cut1):length(A_rot),:) =[];
64          end
65  end
```

B.4 IntensityAnalysisFinal

```
1  clear all
2  close all
3
4  FolderName = 'Alexandra12072016';
5
6  FullPath = [FolderName '/*.tif'];
7  FileInfoAll = dir(FullPath); % gives out a structure containing
       names and other information about all files contained in the
       given folder
8
9  rangeN = 40;
10 rangeMovAvg = 5; %sets the range of the moving average along x
11 x_threshold_max = 130 ;%round(5*length(A)/6); % sets the upper
       threshold in column number to which maxima of the MovStdDev
       are found
12 prom_threshold_tot = 50;
13
14 for v=1:length(FileInfoAll)
15     if mod(v,2) == 1
16         count=1;
17         for w=v:v+1
```

```
18              FileInfoCurrent = FileInfoAll(w); % gives out a
                    structure containing information about file i
19              FileNameCurrent = FileInfoCurrent.name; % gives out
                    a string containg the name of file i
20              FileIn = strcat(FolderName,'/',FileNameCurrent); %
                    generates the complete path of file i
21
22              %% Reading in image file as matrix and plotting it
                    %%
23
24              Im = imread(FileIn); % reads the pixel values into a
                     matrix
25              Im = double(Im);
26
27              Im = ImageRotationFunc(Im,0); % Calls the function
                    to rotate and crop the image/matrix. Second
                    passing argument is the rotation angle
28              Im = fliplr(Im);
29              A(:,:,count) = Im;
30              count=count+1;
31          end
32
33          %% Calculate Correlation
34
35          for i=1:length(A)
36              for j=1:length(A)
37                  corr(i,j) = corr2(A(i,:,1),A(j,:,2));
38              end
39          end
40
41          for i=1:length(A)
42              for j=1:length(A)
43                  if corr(i,j) == max(max(corr))
44                      corrLine = [i,j];
45                  end
46              end
47          end
48
49          Im_merged = [A(:,:,1); A(:,:,2)];
50          Im_merged(corrLine(1):length(A),:) = [];
51          Im_merged(corrLine(1)+1:corrLine(1)+corrLine(2),:) = [];
52
53
54          figure
55          imagesc(Im_merged)
56          colormap(gray)
57
58              %% Calculates the Running Standard Deviation Matrix
```

```
        with a given range (+/- in column) %%
59      for w=1:2
60          MovStdDevMtx = zeros(length(A),length(A)); %
                generating matrix which is to contain the
                standard deviation of its sorrounding column
                entries
61          rangeMovStdDev = 5; % setting range which is taken
                into account for the moving standard deviation
62
63          for i=1:length(A) % i is variable for column number
64              for j=1:length(A) % j is variable for row number
65                  m = 1;
66                  % The following loops (within the if
                        statements) are
67                  % writing the martix entries in A which
                        contained in the
68                  % current range to vecCur_MovStdDev and
                        subsqly caclulate
69                  % the corresponding std dev and write it to
                        MovStdDevMtx
70
71                  if j<=rangeMovStdDev % special case, top
                        boundary
72                      for k=1:(j+rangeMovStdDev)
73                          vecCur_MovStdDev(m,1) = A(k,i,w);
74                          m = m+1;
75                      end
76                      MovStdDevMtx(j,i) = std(vecCur_MovStdDev
                            );
77
78                  elseif j>(length(A)-rangeMovStdDev) %
                        special case, bottom boundary
79                      for k=(j-rangeMovStdDev):length(A)
80                          vecCur_MovStdDev(m,1) = A(k,i,w);
81                          m = m+1;
82                      end
83                      MovStdDevMtx(j,i) = std(vecCur_MovStdDev
                            );
84
85                  else % normal case: rangeMovStdDev number of
                        elements available to top andd bottom
86                      for k=(j-rangeMovStdDev):(j+
                            rangeMovStdDev) % k is vairable for
                            row number within the range
87                          vecCur_MovStdDev(m,1) = A(k,i,w);
88                          m = m+1;
89                      end
90                      MovStdDevMtx(j,i) = std(vecCur_MovStdDev
```

```
                                    );
91                          end
92                      end
93                  end
94
95                  %% Finding the maxima of the Moving Standard
                        Deviation Matrix and plotting them into the image
                        %%
96
97                  LocalMaxStd = vision.LocalMaximaFinder; % calling
                        the maximum finder function
98                  LocalMaxStd.MaximumNumLocalMaxima = 5000; % setting
                        the number of maxima to be found
99                  LocalMaxStd.NeighborhoodSize = [1 1]; % defining the
                         neighbourhoodsize in which only one maximum can
                        be found
100                 LocalMaxStd.Threshold = 1.5*mean(mean(MovStdDevMtx))
                        ; % definig the threshold which a matrix entry
                        has to match or exceed to be a maximum (higher
                        than the mean)
101
102                 locationMaxStd = step(LocalMaxStd, MovStdDevMtx(:,1:
                        x_threshold_max)); % applying the maximum finder
                        with defined settings to the moving standard
                        deviation matrix (within defined thresholds) to
                        find the boundaries of the device/channels/posts
103                 locationMaxStd = double(locationMaxStd);
104
105                 for i=1:length(locationMaxStd) % writes x and y
                        values of the found maxima into separate vectors
106                     locationMaxStd_x(i,1) = locationMaxStd(i,1);
107                     locationMaxStd_y(i,1) = locationMaxStd(i,2);
108                 end
109
110                 hist_x = hist(locationMaxStd_x,(x_threshold_max)); %
                        calculates a histogram of the x occurences of the
                         maxima of the moving standard deviation
111
112                 % Idea: With the previous procedure the coordinates
                        outlet channel boundaries can be found. A
                        histogram of their x coordinates will show a
                        significat drop where the posts
113                 % begin since there are a few columns which are
                        neither interrupted
114                 % by outlet channels nor by posts, i.e. the moving
                        standard
115                 % deviation is quite low. Thus, subsqly this peak
                        has to be found.
```

```
116
117             %% moving average over histogram %%
118
119             % For this, a moving average over the histogram is
                    calculated to
120             % make the peak identification easier.
121
122             MovAvgVec = RunningAvg(hist_x,rangeMovAvg);
123
124             %% Identify peaks in Moving average and read out
                    most prominent peak %%
125
126             [pks_max, locs_max, width_max, prom_max] = findpeaks
                    (MovAvgVec);
127
128             for i=1:length(locs_max)-1
129                 if locs_max(i) <=  prom_threshold_tot &&
                        locs_max(i+1)> prom_threshold_tot
130                     prom_threshold_rel = i+1;
131                 elseif locs_max(1)>=prom_threshold_tot
132                     prom_threshold_rel = 1;
133                 end
134             end
135
136             k = prom_max(prom_threshold_rel);
137
138             for i=prom_threshold_rel:length(prom_max)
139                 if prom_max(i) >= k
140                     promMax = locs_max(i);% promMax is x value
                            of most prominent peak in MovAvgVec (
                            moving averaged histogram of x position
                            maxima of moving standard deviation)
141                     k = prom_max(i);
142                 end
143             end
144
145             plot_promMax = zeros(length(A),2); % plot_promMax is
                    simple vector for line plot of promMax position
                    in A
146
147             for i=1:length(A)
148                 plot_promMax(i,2)=i;
149                 plot_promMax(i,1)=promMax;
150             end
151
152             %% Find column with highest intensity in
                    neighbourhood of most prominent peak position %
153
```

```
154             % It is assumed that one property of the outlet
                    boundary column is
155             % a high mean/median (since no interruptions). Also,
                     the promMax is
156             % in close proximity to the outlet boundary. Thus,
                    the
157             % neighbourhood of promMax is search for the columnn
                     with highest
158             % intensity. This column is assumed to be the
                    boundary column,
159             % boundPos.
160
161             boundPos = 0;
162
163             meanN = zeros(1,2*rangeN+1);
164             j = 1;
165
166             if (promMax + rangeN) > length(A) % adjusting the
                    range of neighbourhood value if promMax is too
                    close to the edge to allow for the preassigned
                    value
167                 for i=(promMax-rangeN):length(A) % calculating
                        the mean of each column within the defined
                        neighbourhood of promMax and assigning it to
                        the vector meanN
168                     meanN(1,j) = mean(A(:,i,w));
169                     j = j+1;
170                 end
171             elseif (promMax - rangeN) < 1
172                 for i=1:(promMax+rangeN) % calculating the mean
                        of each column within the defined
                        neighbourhood of promMax and assigning it to
                        the vector meanN
173                     meanN(1,j) = mean(A(:,i,w));
174                     j = j+1;
175                 end
176             else
177                 for i=(promMax-rangeN):(promMax+rangeN) %
                        calculating the mean of each column within
                        the defined neighbourhood of promMax and
                        assigning it to the vector meanN
178                     meanN(1,j) = mean(A(:,i,w));
179                     j = j+1;
180                 end
181             end
182
183
184             for i=1:length(meanN) % finding the coulun in
```

```
                %defined neighbourhood with largest mean and
                %assigning its x value in A to boundPos
185             if meanN(i) == max(meanN)
186                 if (promMax - rangeN) < 1
187                     boundPos = i;
188                 else
189                     boundPos = promMax - rangeN -1 + i;
190                 end
191             end
192         end
193
194         plot_boundPos = zeros(length(A),2);
195
196         for i=1:length(A)
197             plot_boundPos(i,2)=i;
198             plot_boundPos(i,1)=boundPos;
199         end
200
201         postDist = 22.30;
202
203         rowsBefore = 7;
204         plot_RowsBefore = zeros(length(A),2);
205
206         for i=1:length(A)
207             plot_rowsBefore(i,1) = boundPos + round(
                    rowsBefore*postDist);
208             plot_rowsBefore(i,2) = i;
209         end
210
211         Int(:,:,w) = A(:,(boundPos + round(rowsBefore*
                postDist)),w);
212
213         % background adjustment
214
215         if mod(w,2) == 0
216             back_top = mean(mean(A(corrLine(1):end,boundPos:
                    end,w)));
217         else
218             back_bottom = mean(mean(A(1:corrLine(2),boundPos
                    :end,w)));
219         end
220
221
222         %% Plots %%
223
224         FileNameCurrent = strrep(FileNameCurrent,'_','');
225         FileNameCurrent = strrep(FileNameCurrent,'
                SubtractedAveraged','');
```

```
226             FileNameCurrent = strrep(FileNameCurrent,'outlet','')
                    ;
227             FileNameCurrent = FileNameCurrent(1:end-7);
228
229             if mod(w,2) == 0
230                 FileNameCurrent = strcat(FileNameCurrent, 'rTop'
                        );
231             else
232                 FileNameCurrent = strcat(FileNameCurrent, '
                        Bottom');
233             end
234
235             figure
236             imagesc(A(:,:,w))
237             colormap(gray)
238             hold on
239             scatter(locationMaxStd(:,1),locationMaxStd(:,2),'.r'
                    ) % plot the found maxima as scatter plot
240             title('Found maxima of moving StdDev')
241
242             figure
243             plot(hist_x)
244             grid on
245             title('Histogram of x-value occurences for maxima of
                    MovStdDev')
246
247             figure
248             plot(MovAvgVec)
249             hold on
250             scatter(locs_max,pks_max)
251             hold on
252             scatter(locs_max,prom_max)
253             grid on
254             legend('Moving average','found peaks','prominence','
                    Location','NorthWest')
255             title('Moving average over histogram of x-value
                    occurences for maxima of MovStdDev incl
                    identified peaks')
256
257
258             figure
259             imagesc(A(:,:,w))
260             colormap(gray)
261             hold on
262             plot(plot_promMax(:,1),plot_promMax(:,2),'LineWidth'
                    ,1.5)
263             hold on
264             plot(plot_boundPos(:,1),plot_boundPos(:,2),'
```

```
                LineWidth',1.5)
265             hold on
266             plot(plot_rowsBefore(:,1),plot_rowsBefore(:,2),'
                    LineWidth',1.5)
267             legend('Maximum prominence peak','Device boundary','
                    7 rows before outlet','Location','SouthEast')
268             saveas(gcf,strcat(FolderName,'\',FileNameCurrent,'.
                    png'))
269         end
270         Int_bottom = Int(:,:,2);
271         Int_top = Int(:,:,1);
272
273         %% background adjustment
274
275         back_diff = back_top-back_bottom;
276         Int_bottom(:,:) = Int_bottom(:,:) + back_diff;
277
278         Int_merged = [Int_top; Int_bottom];
279         Int_merged(corrLine(1):length(A)) = [];
280         Int_merged(corrLine(1)+1:corrLine(1)+corrLine(2)) = [];
281
282         figure
283         plot(smooth(Int_merged,3))
284         grid on
285         xlabel('Pixel number from top to bottom')
286         ylabel('Intensity')
287
288
289         FileIntensity = FileIn(1:end-7);
290         FileIntensityTxt = strcat(FileIntensity,'Intensity.txt')
                ;
291         FileIntensityPng = strcat(FileIntensity,'Intensity.png')
                ;
292
293         dlmwrite(FileIntensityTxt,Int_merged);
294
295         [pks_Int,locs_pks_Int] = findpeaks(Int_merged);
296         saveas(gcf,FileIntensityPng)
297     end
298 end
```

Appendix C

Image J macros

C.1 GenerateParticleTracks

```
1  macro "GenerateParticleTracks" {
2          open();
3          Stack.getDimensions(width, height, channelCount,
               sliceCount, frameCount);
4          TitleStack = getTitle();
5          filenameDir = getDirectory("image");
6          numberAvgFrames = 4;
7
8          for (i = 1; i <= frameCount; i+=numberAvgFrames){
9                          j = (i+numberAvgFrames-1);
10                         run("Z Project...", "start=i stop=j
                               projection=[Max Intensity]");
11                         filenameSave = filenameDir + TitleStack
                               + "_Max_" +  i + "_" + j;
12                         save(filenameSave);
13                         close();
14                         selectWindow(TitleStack);
15
16         }
17 }
```

Bibliography

[1] Lonza. Detection and Sizing of DNA in Agarose Gels. http://bio.lonza.com/uploads/tx_mwaxmarketingmaterial/Lonza_BenchGuides_SourceBook_Section_IV_-_Detection_and_Sizing_of_DNA_in_Agarose_Gels.pdf. [Online; accessed 06-May-2016].

[2] J Han and H G Craighead. Separation of long DNA molecules in a microfabricated entropic trap array. *Science*, 288(5468):1026–1029, 2000.

[3] A Lenshof and T Laurell. Continuous separation of cells and particles in microfluidic systems. *Chemical Society Reviews*, 39(3):1203–1217, 2010.

[4] A L Paguirigan and D J Beebe. Microfluidics meet cell biology: bridging the gap by validation and application of microscale techniques for cell biological assays. *BioEssays*, 30(9):811–821, 2008.

[5] P Sajeesh and A K Sen. Particle separation and sorting in microfluidic devices: a review. *Microfluidics and Nanofluidics*, 17(1):1–52, 2014.

[6] L R Huang, E C Cox, R H Austin, and J C Sturm. Continuous particle separation through deterministic lateral displacement. *Science (New York, N.Y.)*, 304(5673):987–990, 2004.

[7] Y Chen, E S Abrams, T C Boles, J N Pedersen, H Flyvbjerg, R H Austin, and J C Sturm. Concentrating Genomic Length DNA in a Microfabricated Array.

[8] F Persson and J O Tegenfeldt. DNA in nanochannels—directly visualizing genomic information. *Chemical Society Reviews*, 39(3):985, 2010.

[9] L Pray. Discovery of DNA structure and function: Watson and Crick. *Nature Education*, 1(1), 2008.

[10] M Mandelkern, J G Elias, D Eden, and D M Crothers. The dimensions of DNA in solution. *Journal of molecular biology*, 152(1):153–161, 1981.

[11] Genome, Genome size. https://en.wikipedia.org/wiki/Genome. [Online; accessed 08-May-2016].

[12] P Nelson. *Biological physics*. WH Freeman New York, 2004.

[13] L K Nyberg. *Development of methods for optical mapping of nanoconfined DNA*. PhD thesis, Chalmers University of Technology, 2015.

[14] J F Marko and E D Siggia. Stretching DNA. *Macromolecules*, 28(26):8759–8770, 1995.

[15] W Reisner, J N Pedersen, and R H Austin. DNA confinement in nanochannels: physics and biological applications. *Reports on Progress in Physics*, 75(10):106601, 2012.

[16] M Daoud and P-G De Gennes. Statistics of macromolecular solutions trapped in small pores. *Journal de Physique*, 38(1):85–93, 1977.

[17] A Muralidhar, D R Tree, Y Wang, and K D Dorfman. Interplay between chain stiffness and excluded volume of semiflexible polymers confined in nanochannels. *The Journal of chemical physics*, 140(8):084905, 2014.

[18] J O Tegenfeldt, C Prinz, H Cao, S Chou, W W Reisner, R Riehn, Y M Wang, E C Cox, J C Sturm, P Silberzan, et al. The dynamics of genomic-length DNA molecules in 100-nm channels. *Proceedings of the National Academy of Sciences of the United States of America*, 101(30):10979–10983, 2004.

[19] T Odijk. The statistics and dynamics of confined or entangled stiff polymers. *Macromolecules*, 16(8):1340–1344, 1983.

[20] D R Tree, Yi Wang, and K D Dorfman. Extension of DNA in a nanochannel as a rod-to-coil transition. *Physical review letters*, 110(20):208103, 2013.

[21] E Werner and B Mehlig. Confined polymers in the extended de gennes regime. *Physical Review E*, 90(6):062602, 2014.

[22] L Dai, J van der Maarel, and P S Doyle. Extended de gennes regime of DNA confined in a nanochannel. *Macromolecules*, 47(7):2445–2450, 2014.

[23] P-G De Gennes. Coil-stretch transition of dilute flexible polymers under ultrahigh velocity gradients. *The Journal of Chemical Physics*, 60(12):5030–5042, 1974.

[24] T T Perkins, S R Quake, D E Smith, and S Chu. Relaxation of a single DNA molecule observed by optical microscopy. *Science (New York, N.Y.)*, 264(5160):822–826, 1994.

[25] T T Perkins, D E Smith, R Larson, and S Chu. Streching of a Single Tethered Polymer in a Uniform Flow, 1995.

[26] S Manneville, P Cluzel, J-L Viovy, D Chatenay, and F Caron. Evidence for the universal scaling behaviour of a freely relaxing DNA molecule. *Europhysics Letters (EPL)*, 36(6):413–418, 1996.

[27] T T Perkins, D E Smith, and S Chu. Single polymer dynamics in an elongational flow. *Science (New York, N.Y.)*, 276(5321):2016–21, 1997.

[28] S W P Turner, M Cabodi, and H G Craighead. Confinement-induced entropic recoil of single DNA molecules in a nanofluidic structure. *Physical Review Letters*, 88(12):128103, 2002.

[29] D E Smith and S Chu. Response of flexible polymers to a sudden elongational flow. *Science*, 281(5381):1335–1340, 1998.

[30] S B Smith, L Finzi, and C Bustamante. Direct mechanical measurements of the elasticity of single DNA molecules by using magnetic beads. *Science*, 258(5085):1122–1126, 1992.

[31] O B Bakajin, T A J Duke, C F Chou, S S Chan, R H Austin, and E C Cox. Electrohydrodynamic Stretching of DNA in Confined Environments. pages 2737–2740, 1998.

[32] S M J L Wildenberg, B Prevo, and E J G Peterman. *Single Molecule Analysis: Methods and Protocols*, chapter A Brief Introduction to Single-Molecule Fluorescence Methods, pages 81–99. Humana Press, Totowa, NJ, 2011.

[33] H Mühlpfordt. Schematic of a fluorescence microscope. https://en.wikipedia.org/wiki/File:FluorescenceFilters_2008-09-28.svg. [Online; accessed 15-Apr-2016].

[34] H S Rye, S Yue, D E Wemmer, M A Quesada, R P Haugland, R A Mathies, and A N Glazer. Stable fluorescent complexes of double-stranded DNA with bis-intercalating asymmetric cyanine dyes: properties and applications. *Nucleic acids research*, 20(11):2803–2812, 1992.

[35] ThermoFisher Scientific. Product Information YOYO-1 Iodide (491/509). https://www.thermofisher.com/order/catalog/product/Y3601?ICID=search-product. [Online; accessed 09-Apr-2016].

[36] B Kundukad, J Yan, and P S Doyle. Effect of YOYO-1 on the mechanical properties of DNA. *Soft matter*, pages 9721–9728, 2014.

[37] K Günther, M Mertig, and R Seidel. Mechanical and structural properties of YOYO-1 complexed DNA. *Nucleic acids research*, 38(19):6526–6532, 2010.

[38] M Maaloum, P Muller, and S Harlepp. DNA-intercalator interactions: structural and physical analysis using atomic force microscopy in solution. *Soft Matter*, 9(47):11233–11240, 2013.

[39] J P Beech. *Microfluidics Separation and Analysis of Biological Particles*. PhD thesis, Lund University, 2011.

[40] H Bruus. Lecture notes, Theoretical microfluidics. http://homes.nano.aau.dk/lg/Lab-on-Chip2008_files/HenrikBruus_Microfluidics%20lectures.pdf, 2006. [Online; accessed 25-Apr-2016].

[41] J McGrath, M Jimenez, and H Bridle. Deterministic lateral displacement for particle separation: a review. *Lab on a chip*, 14(21):4139–58, 2014.

[42] J P Brody, P Yager, R E Goldstein, and R H Austin. Biotechnology at low Reynolds numbers. *Biophysical journal*, 71(6):3430, 1996.

[43] J A Davis. *Microfluidic Separation of Blood Components through Deterministic Lateral Displacement* . PhD thesis, Princeton University, 2008.

[44] J Wei, H Song, Z Shen, Y He, X Xu, Y Zhang, and B N Li. Numerical Study of Pillar Shapes in Deterministic Lateral Displacement Microfluidic Arrays for Spherical Particle Separation. *IEEE Transactions on Nanobioscience*, 14(6):660–667, 2015.

[45] K Loutherback, K S Chou, J Newman, J Puchalla, R H Austin, and J C Sturm. Improved performance of deterministic lateral displacement arrays with triangular posts. *Microfluidics and nanofluidics*, 9(6):1143–1149, 2010.

[46] K K Zeming, Si Ranjan, and Y Zhang. Rotational separation of non-spherical bioparticles using i-shaped pillar arrays in a microfluidic device. *Nature communications*, 4:1625, 2013.

[47] S H Holm, J P Beech, M P Barrett, and J O Tegenfeldt. Separation of parasites from human blood using deterministic lateral displacement. *Lab on a chip*, 11(7):1326–1332, 2011.

[48] J P Beech, S H Holm, K Adolfsson, and J O Tegenfeldt. Sorting cells by size, shape and deformability. *Lab on a Chip*, 12(6):1048, 2012.

[49] E A DiMarzio and C M Guttman. Separation by flow. *Macromolecules*, 3(2):131–146, 1970.

[50] Y Xia and G M Whitesides. Soft Lithography. *Annual Review in Material Science*, 28(12):153–184, 1998.

[51] C Iliescu, H Taylor, M Avram, J Miao, and S Franssila. A practical guide for the fabrication of microfluidic devices using glass and silicon. *Biomicrofluidics*, 6(1):016505, 2012.

[52] J E Mark, H R Allcock, and R West. *Inorganic polymers*. Oxford University Press, 2005.

[53] J O Tegenfeldt, C Prinz, H Cao, R L Huang, R H Austin, S Y Chou, E C Cox, and J C Sturm. Micro- and nanofluidics for DNA analysis. *Anal. Bioanal. Chem.*, 378(7):1678–1692, 2004.

[54] F Brochard and P-G de Gennes. Dynamics of confined polymer chains. *The Journal of Chemical Physics*, 67(1):52–56, 1977.

[55] L Guo and F Gai. Simple method to enhance the photostability of the fluorescence reporter R6G for prolonged single-molecule studies. *The Journal of Physical Chemistry A*, 117(29):6164–6170, 2013.

[56] J R Wenner, M C Williams, I Rouzina, and V A Bloomfield. Salt dependence of the elasticity and overstretching transition of single dna molecules. *Biophysical journal*, 82(6):3160–3169, 2002.

[57] K K Zeming, N V Thakor, Y Zhang, and C-H Chen. Real-time modulated nanoparticle separation with an ultra-large dynamic range. *Lab Chip*, 16(1):75–85, 2016.

[58] Wacker Group. Product Information ELASTOSIL® A07. http://www.wacker.com/cms/en/products/product/product.jsp?product=9010. [Online; accessed 19-Apr-2016].